CHAPTER 5

THE EVOLUTION OF THE MORPHOLOGY AND SURFACE BRIGHTNESS OF SUPERNOVA REMNANTS WITH PULSARS IN THEM

One of the intriguing things about supernova remnants is that there are three distinct types of them: **(a)** plerions with no limb brightening, **(b)** shells with hollow interiors, **(c)** shells with plerionic components at their centres. An interesting question that has been raised in the literature is whether these are remnants of different types of explosions, or whether they represent different stages of evolution.

This chapter is devoted to a quantitative discussion of this important question. The results of model calculations of the evolution of surface brightness and morphology are presented. We show that the morphology'of a supernova remnant will depend upon the velocity of expansion, the density of the ambient medium into which it is expanding, and the parameters of the central pulsar if it is present.

CONTENTS

CHAPTER 5

THE EVOLUTION OF THE MORPHOLOGY AND SURFACE BRIGHTNESS OF SUPERNOVA REMNANTS WITH PULSARS IN THEM

CHAPTER 5

THE EVOLUTION OF THE MORPHOLOGY AND SURFACE BRIGHTNESS OF SUPERNOVA REMNANTS WITH PULSARS IN THEM

5.1 INTRODUCTION

In chapter 2 we discussed the evolution of the luminosity of pulsar-produced nebulae (plerions). These nebulae are characterized by their centre-filled morphology (fig. 5.1a), as opposed to the shell-like appearance of the majority of supernova remnants (fig. 5.1b). A few SNRs also exhibit a hybrid morphology - a shell surrounding a plerion (fig. 5.1c). The emission from a plerionic remnant is believed to be due to fast particles and magnetic field produced by an active central pulsar, as discussed in detail in chapter 2. It has been argued that the radio emission from shell remnants, on the other hand, originates when material ejected in the supernova explosion interacts with the interstellar matter, causing turbulence at the interface. This generates the magnetic field and fast particles necessary for radio emission (Gull 1973, 1975; Scott and Chevalier 1975; Cowsik and Sarkar 1984).

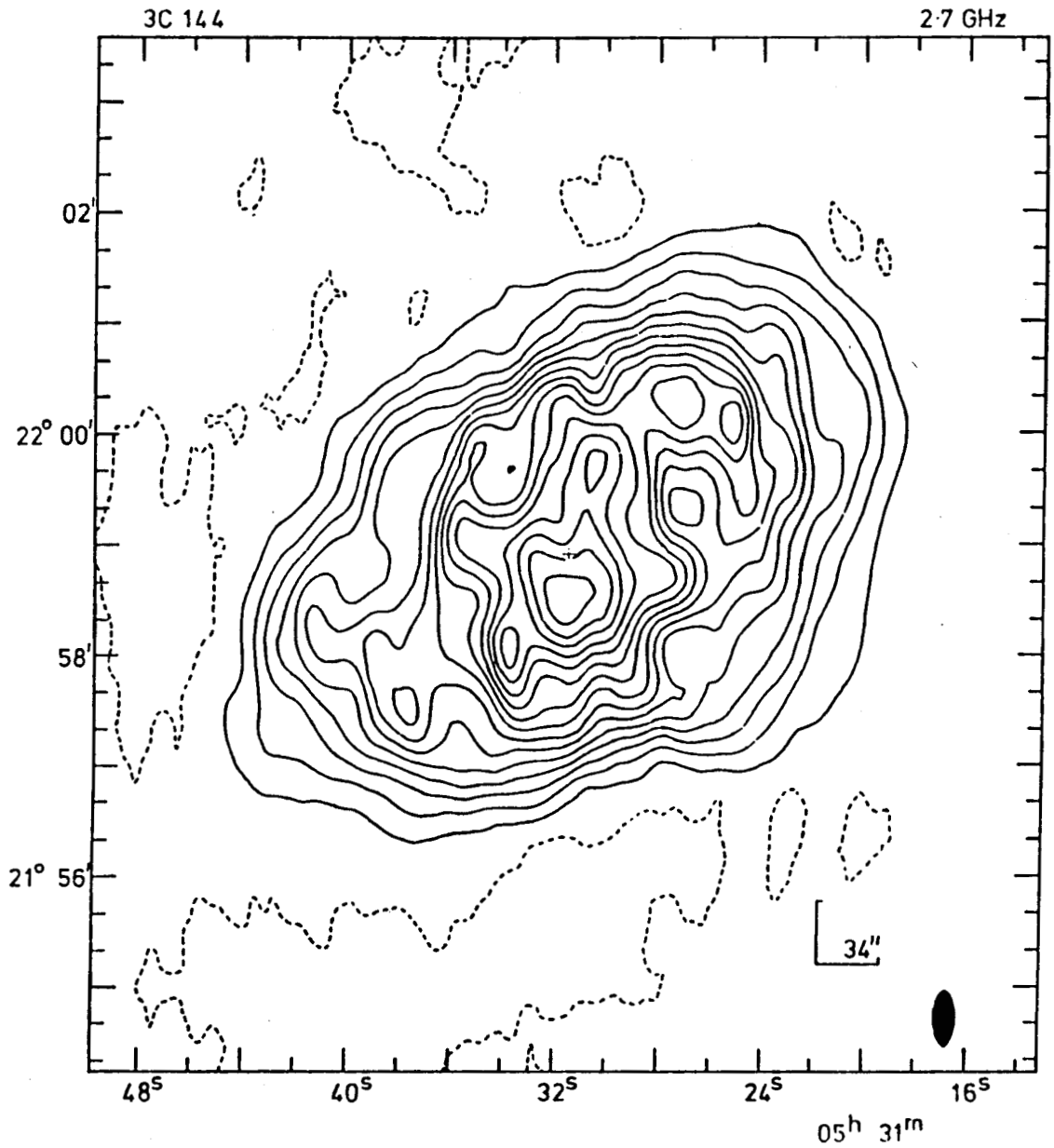

Map of total intensity at 2.7 GHz. The half-pourer beammidth (1 1" x 29" arc) is shown in the bottom right-hand corner. The contotcr interval is 272 °K (0·431 X 10⁻²⁶ W m⁻² Hz⁻¹ (beam area)⁻¹ and coordinates are for epoch 1950·0, as throughout the paper. The cross marks the pulsar.

Fig. 5.1 (a): The Crab Nebula at 2.7 GHz – the prime example of a Plerionic supernova remnant. (Reproduced from Wilson, 1972)

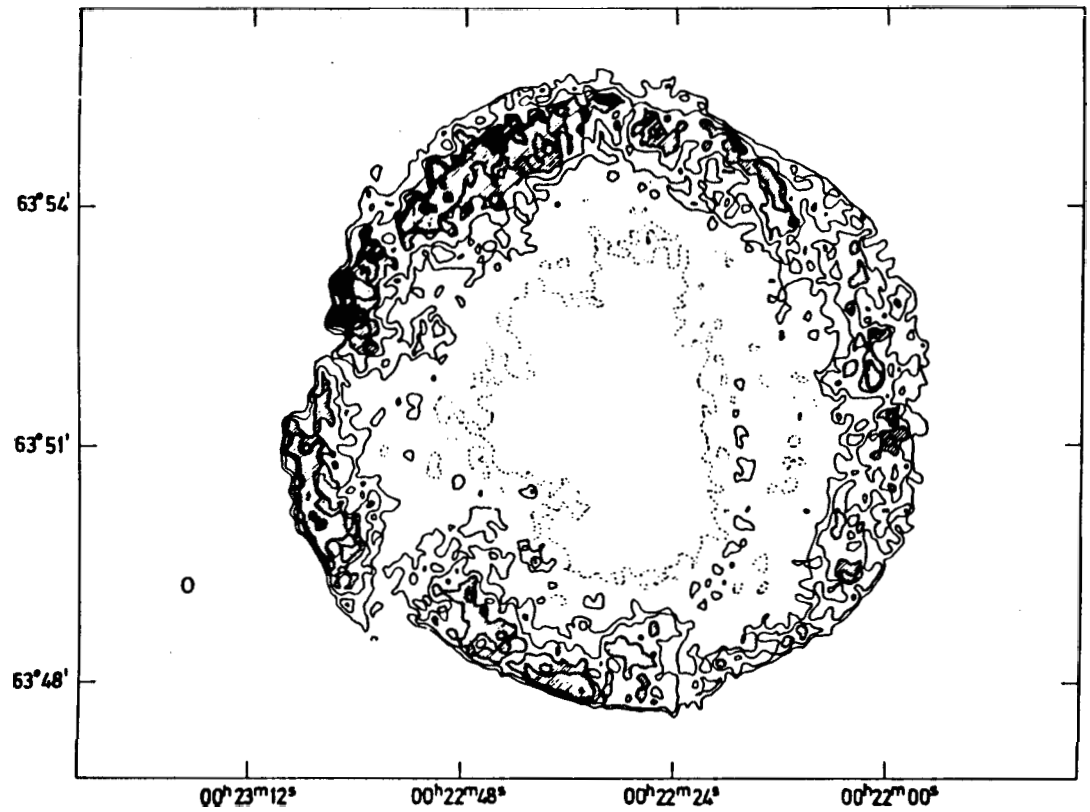

Fig. 5.1 (b): A 4995 MHz map of the remnant of Tycho's supernova (from Duin and Strom 1975). The zero intensity contour is shown dotted. This is a typical shell SNR.

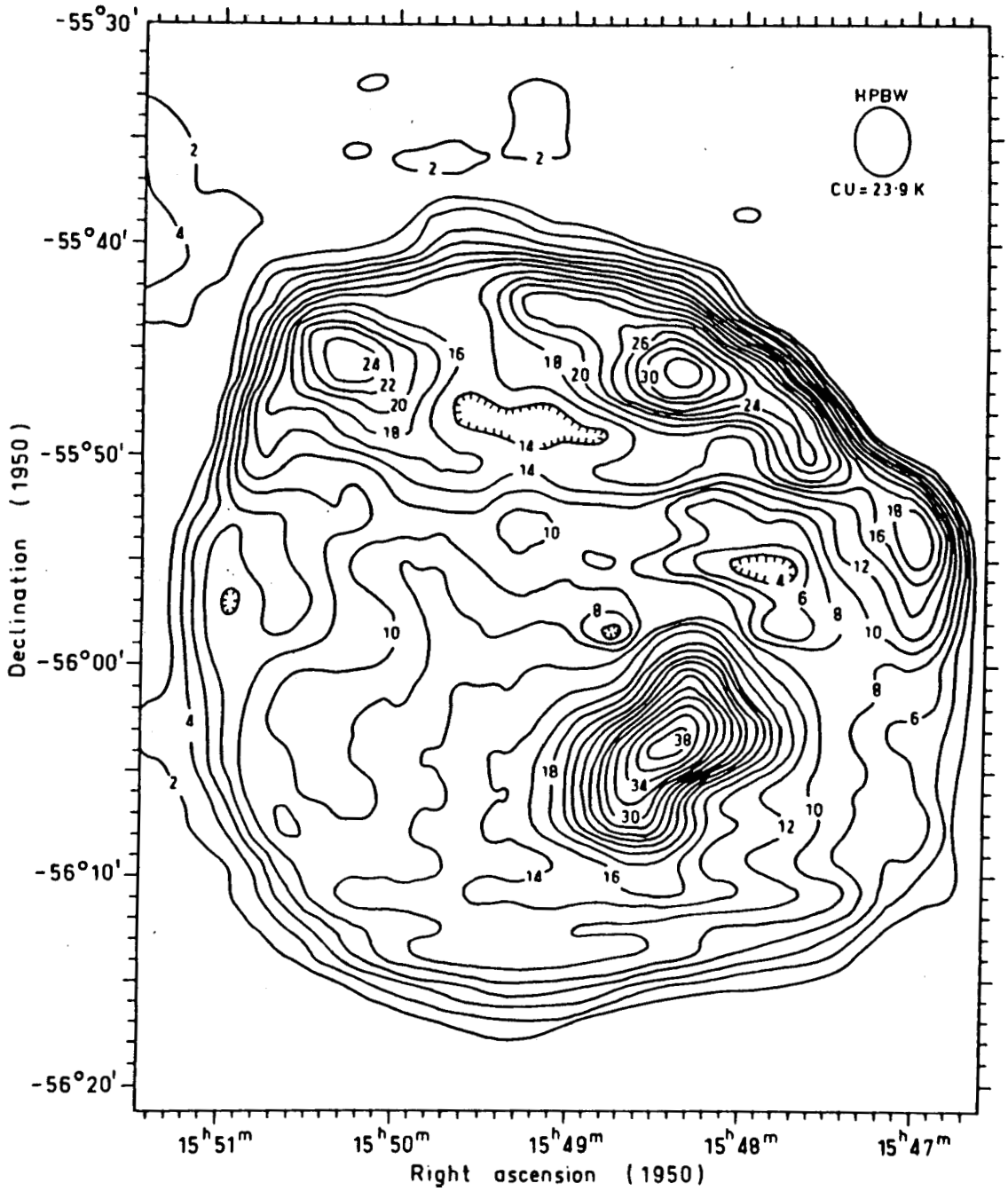

Contour map of G326.3–1.8 (MSH 15–56) at 408 MHz.

Fig. 5.1 (c): An example of a shell-plerion combination – the supernova remnant G326.3-1.8 at 408 MHz. (From Clark et. al. 1975).

It has been suggested in the literature that type I supernovae produce shell SNRs with hollow interiors, since in most current models no stellar remnant is left behind. Others have argued that type II supernovae, which are presumably from massive progenitors, will produce plerions since a neutron star is expected to be left behind (Shklovskii 1980; see also Weiler 1983, 1985). Such a distinction, however, is clearly an oversimplification. While it is reasonable to suppose that those supernovae which do not leave behind pulsars will not produce plerionic nebulae, the presence of a pulsar does not guarantee that the remnant will have a plerionic appearance at all times. The radio luminosity of a plerion will decrease with time, as discussed in chapter 2. As the remnant expands, however, it must sweep up interstellar matter and decelerate, which will cause radio emission to build up in a shell. The overall appearance of a supernova remnant will therefore depend on the relative surface brightness of the plerionic and the shell components. If the plerionic component is much brighter than the shell then we shall see a filled centre remnant like the Crab nebula. The supernova remnant MSH 15-52, a shell remnant containing a pulsar, may be an example of the opposite kind, where the shell emission is much stronger than the plerion.

The luminosity of the plerionic component depends on

- **The initial rotation period and magnetic field of the pulsar, and**
- **The velocity of expansion of the nebula.**

The luminosity of the shell is determined by

- **The energy of the explosion,**
- **The amount of matter ejected, and**
- **The density of the surrounding interstellar matter**

In this chapter we shall study the evolution of both the plerion and the shell components, and discuss the question of the possible change in **morphology** of supernova remnants with age. Although it has,been suggested **(Lozinskaya 1980)** that **SNRs** will have a filled centre morphology in their youth, but gradually turn into hollow shells, this important question has not received much quantitative attention. In sections **5.2** and 5.3 we describe the procedure adopted to compute the evolution of surface brightness of the plerion and the shell component respectively. In section **5.4** we discuss our results. In section 5.5 we present a model for the supernova remnant **0540-69.3** in the Large Magellanic Cloud, in which a pulsar has recently been discovered.

5.2 INTERACTION OF PLERIONS WITH THE INTERSTELLAR MEDIUM

The evolution of the luminosity of a freely expanding plerion has been discussed in chapter 2 and appendix 2.A2. However, a freely expanding plerionic nebula will begin to decelerate when the mass swept up from the interstellar medium becomes comparable to the mass in the ejected material which forms the boundary of the plerion. This change in velocity will cause a change in the adiabatic loss rate of particle and field energy and will thus affect the luminosity evolution of the plerion. Numerical models of plerions in decelerated expansion have been constructed by Reynolds and Chevalier (1984) and Bandiera, Pacini and Salvati (1984). The latter authors have incorporated the deceleration by attributing to the boundary of the plerion an expansion velocity that keeps the total kinetic energy of the ejected plus the swept up matter independent of time. That is, the velocity evolves in such a way that

$$\left[M_{ej} + \frac{4\pi}{3} \rho R^3(t)\right] v^2(t) = \text{constant} \qquad (5.1)$$

where M_{ej} = total mass ejected in the supernova explosion

ρ = mass density of the Interstellar matter, and

$R(t)$ and $v(t)$ are the radius and expansion velocity of the plerion at time t respectively.

At early times, when $M_{ej} \gg \frac{4\pi}{3} R^3(t) \rho$, (5.1) gives a free expansion phase: v =constant. Much later, when $\frac{4\pi}{3} R^3(t) \gg M_{ej}$, then the same expression gives

$R \propto t^{0.4}$, the expansion law appropriate for a Sedov blast wave. We shall use here a similar model for nebular expansion. Let t_o be the time when the swept up mass and the ejected mass are equal, i.e.

$$\frac{4\pi}{3} R^3(t_o)\, \rho = M_{ej}. \tag{5.2}$$

We shall in the present case approximate the nebular expansion as

$$\left.\begin{aligned} R &= vt \quad \text{for} \quad t < t_o \\ \text{and} \quad R &= v t_o \left(t/t_o\right)^{0.4} \quad \text{for } t > t_o. \end{aligned}\right\} \tag{5.3}$$

A similar approximation for R(t) was used by Weiler and Panagia (1980) to examine the behaviour of the radio luminosity of a plerion in decelerated expansion. Their treatment, however, was limited because they considered the evolution only of the very lowest energy particles which may not be relevant for emission at the desired frequencies, and also because of the fact that they considered t_o to be equal to the initial spindown timescale of the pulsar - which is not necessarily true.

In an appendix at the end of this chapter (Appendix 5.A1) we derive the time dependence of the magnetic field and particle distribution of a plerion experiencing deceleration: $R \propto t^{\eta}, \eta < 1$. It is shown there that the particle spectrum is divided into several energy ranges with different power-law indices.

The spectral luminosity at a given frequency ν is then obtained from the particle distribution and magnetic field **B(t)** as follows:

- The energy $E(\nu,t)$ of the particles radiating at frequency ν is given by

$$E(\nu,t) = \left[\nu / c_2 B(t)\right]^{1/2} \qquad (5.4)$$

where $c_2 = 1.82 \times 10^{18}$ **Hz/gauss/erg^2**

- The number of particles **N(E,t)** in unit energy interval around **E(ν,t)** is then computed from the appropriate relation given in appendix **5.A1.**

- The luminosity $L_\nu(t)$ is then computed from* :

$$L_\nu(t) = \frac{c_1}{2c_2} B(t)\, E(\nu,t)\, N(E,t) \qquad (5.5)$$

where $c_1 = 2.37 \times 10^{-3}$ **gauss^{-2}** erg^{-1} s^{-1}

The above relation results from the monochromatic approximation for the synchrotron radiation from a single electron:

$$P(\nu,E) = c_1 B^2 E^2 \delta(\nu - c_2 B E^2).$$

- The average surface brightness of the plerion can then be obtained from:

$$\Sigma_\nu(t) = L_\nu(t) / 4\pi^2 R^2(t)$$

where **R(t)** is the radius of the nebula at time t.

---

* In the early phase of evolution the radio emission will be affected by synchrotron self-absorption, and the value of L_ν has to be modified accordingly. In our model calculations we have taken this into account.

5.3 THE SHELL COMPONENT

Let us now turn our attention to the boundary of the plerion, where the swept up matter is accumulating resulting in the deceleration discussed above. This question has been discussed by several authors in the context of the deceleration of the supernova blast wave. In this section we shall summarize the relevant physics, as well as the procedure to calculate the expected radio emission from such a decelerating boundary.

The relativistic electrons and magnetic field in the postshock region of a shell supernova remnant cannot be attributed to the initial explosion alone since adiabatic losses would have reduced their energies far below that required to maintain the observed luminosity. It is therefore necessary to have continued acceleration of relativistic particles and generation of magnetic field in this region. Numerical fluid dynamic models studied by Gull (1973), suggest a plausible mechanism for the generation of strong magnetic fields and relativistic particles in the postshock region in supernova remnants. His simulations showed that the interaction between the interstellar medium and the expanding ejecta leads to a convective instability in a narrow zone behind the shock. About $\sim 1\%$ of the total energy of the supernova remnant goes into turbulence in this zone. These turbulent cells can amplify pre-existing magnetic field by twisting and tangling the field lines. Charged particles can be accelerated by the Fermi process in this turbulent region.

A rough equipartition may be reached between the energy densities in turbulence, magnetic field and relativistic particles. This is sufficient to account for observed radio luminosity of supernova remnants. Detailed models of particle acceleration in the convection zone were considered by Sarkar (1982) leading to similar conclusions. In what follows we shall also adopt the same picture. In addition we shall make the reasonable assumption that relativistic particles from the pulsar-produced nebula do not penetrate into the shell region. Thus the development of the shell and the plerion components will be essentially independent.

Gull (1973) has presented in graphical form the development of the magnetic field B_s and the turbulent energy E_{turb} as a function of time within the convection zone (fig. 5.2). These were calculated with the model parameters:

Energy of the blast $E_{tot} = 10^{51}$ ergs

Mass ejected $M_{ej} = 10^{33}$ gm

Density of ambient medium $n_o = 1$ H Atom/cc.

To use these results in our models we adopt the following procedure. Using the radius vs. time relation in Gull's models we express $\frac{E_{turb}}{E_{tot}}$ and $B_s\left(\frac{M_{ej}}{n_o E_{tot}}\right)^{1/2}$ as a function of mass ratio x, defined as the ratio of swept up mass to ejected mass:

$$x(t) \equiv \frac{\frac{4\pi}{3} R^3(t)\, n_o m_p}{M_{ej}} \quad ; \quad y(t) \equiv \log x(t) \qquad (5.6)$$

where $R(t)$ is the SNR radius as a function of time and m_p is the proton mass.' From the plots presented by Gull, we

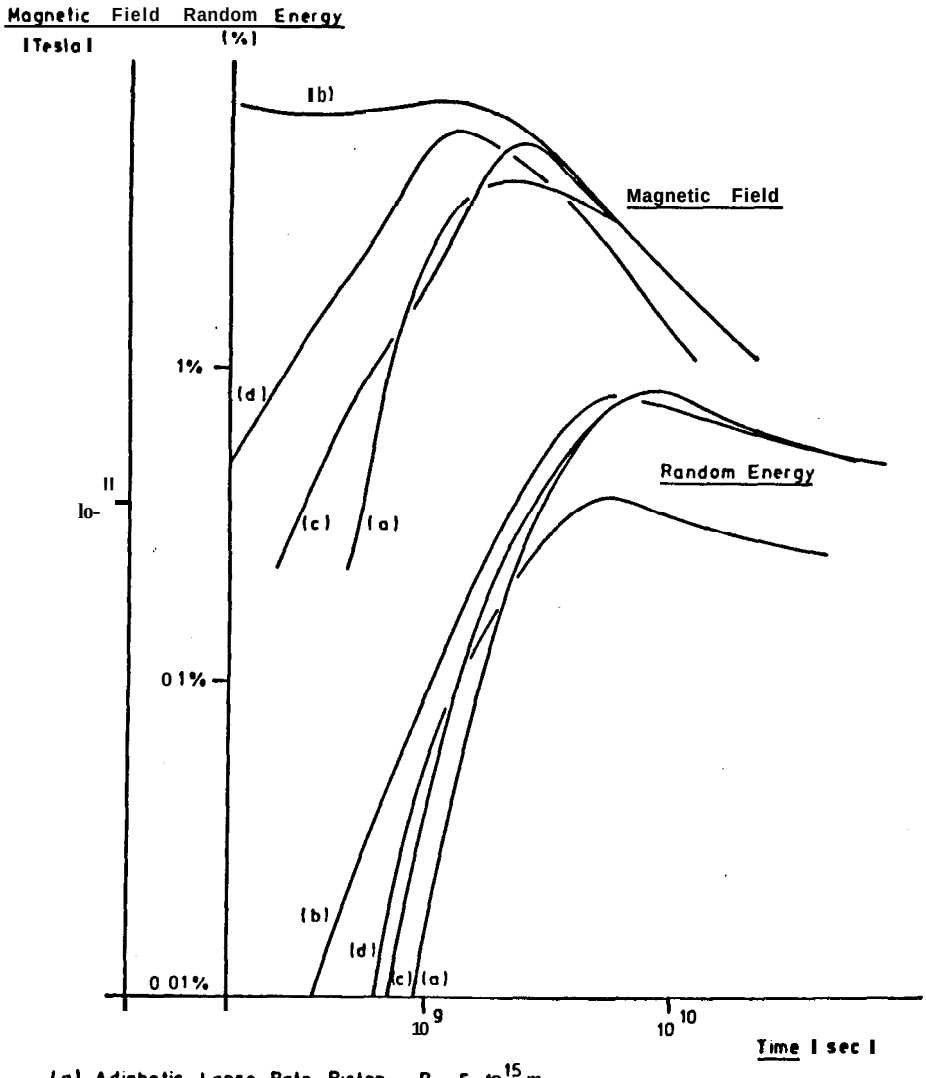

(a) Adiabatic Lapse Rate Piston, $R_o = 5 \times 10^{15}$ m.
(b) Adiabatic Lapse Rate Piston, $R_o = 5 \times 10^{14}$ m
(c) Constant Density Piston
(d) Isothermal Piston

. *Turbulent energy a d magnetic field in the convection zone. Note that, whilst the individual piston models show great differences in the early part of the evolution (particularly for small Ro) the predicted turbulent energies and magnetic fields agree to within a factor of 2 when the mass ratio is greater than 0·1 ($t > 10^9$ s).*

Fig. 5.2: The evolution of magnetic field and the energy in random motions in the turbulent zone of a supernova remnant, as presented by Gull (1973). The energy in turbulence is given in units of the total blast energy. The results are shown for different piston models used by Cull. For the sake of definiteness, we have used the results of piston model (c) in all our model calculations.

obtained the turbulent energy and magnetic field as a function of time. Values of x at these times were then obtained using his radius vs. time plots. Thus the turbulent energy and the magnetic field were expressed as functions of the mass ratio. According to the scaling relations in Gull's model, the value of E_{turb} at a given mass ratio is proportional to the total energy E_{tot} and the magnetic field at a given mass ratio is proportional to $\left(\frac{n_o E_{tot}}{M_{ej}}\right)^{1/2}$. Thus the dependence of turbulent energy and magnetic field as functions of the mass ratio were expressed in the following best-fit polynomial form for convenient use:

$$\left.\begin{aligned} &\log E_{turb} = \log E_{tot} - 2.177 + 0.637y - 0.025y^2 \\ &\qquad\qquad \text{for } y < 0.15 \\ &\text{and} \\ &\log E_{turb} = \log E_{tot} - 2.114 + 0.076y - 0.130y^2 \\ &\qquad\qquad \text{for } y > 0.15. \end{aligned}\right\} \quad (5.7)$$

$$\left.\begin{aligned} &\log B_s = -2.938 + 0.527y + 0.5\log(E_{51}\, n_o/M_{ej}) \\ &\qquad\qquad \text{for } y < -0.4 \\ &\text{and} \\ &\log B_s = -3.312 - 0.420y - 0.178y^2 + 0.285y^3 \\ &\qquad -0.169y^4 + 0.5\log(E_{51}\, n_o/M_{ej}) \quad \text{for } y > -0.4. \end{aligned}\right\} \quad (5.8)$$

In (5.8) E_{51} stands for $\frac{E_{tot}}{10^{51}\text{ erg}}$ and M_{ej} is in units of solar masses.

In our models, we calculate R(t) from (5.3), and then α and y from (5.6). We write $E_{tot} = \frac{1}{2} M_{ej} V^2$, where , which also appears in equation (5.3), is the expansion velocity at t=0. Using these values, we obtain the magnetic field B_s and particle energy content U_{rel} from (5.8) and (5.7) respectively. Specifying a minimum energy E_{min} of the particle distribution and an energy spectral index $\gamma_s > 2$, the particle distribution is written as

$$N(E,t) = (\gamma_s - 2)\, U_{rel}\, E_{min}^{\gamma_s - 2}\, E^{-\gamma_s} \qquad (5.9)$$

Given a frequency ν of observation, the energy of the radiating particles is found from (5.4), with $B = B_s$. The number of particles N(E) at this energy is then obtained from (5.9) and using these values in (5.5) one obtains the luminosity of the shell component. The average surface brightness of the shell over the projected bright ring of emission is then computed from :

$$\frac{L_\nu}{4\pi^2 R^2} \cdot \frac{(2-\delta)^{1/2}}{\delta^{1/2}(3-3\delta+\delta^2)}$$

where δ is the thickness of the emitting region in units of the radius of the shell. In our model calculations we have used $\delta = 0.2$

5.4 RESULTS

Our results are summarized in figures 5.3 - 5.5 in which we have shown the simultaneous evolution of the surface brightness of the plerion (solid lines) and the overlying

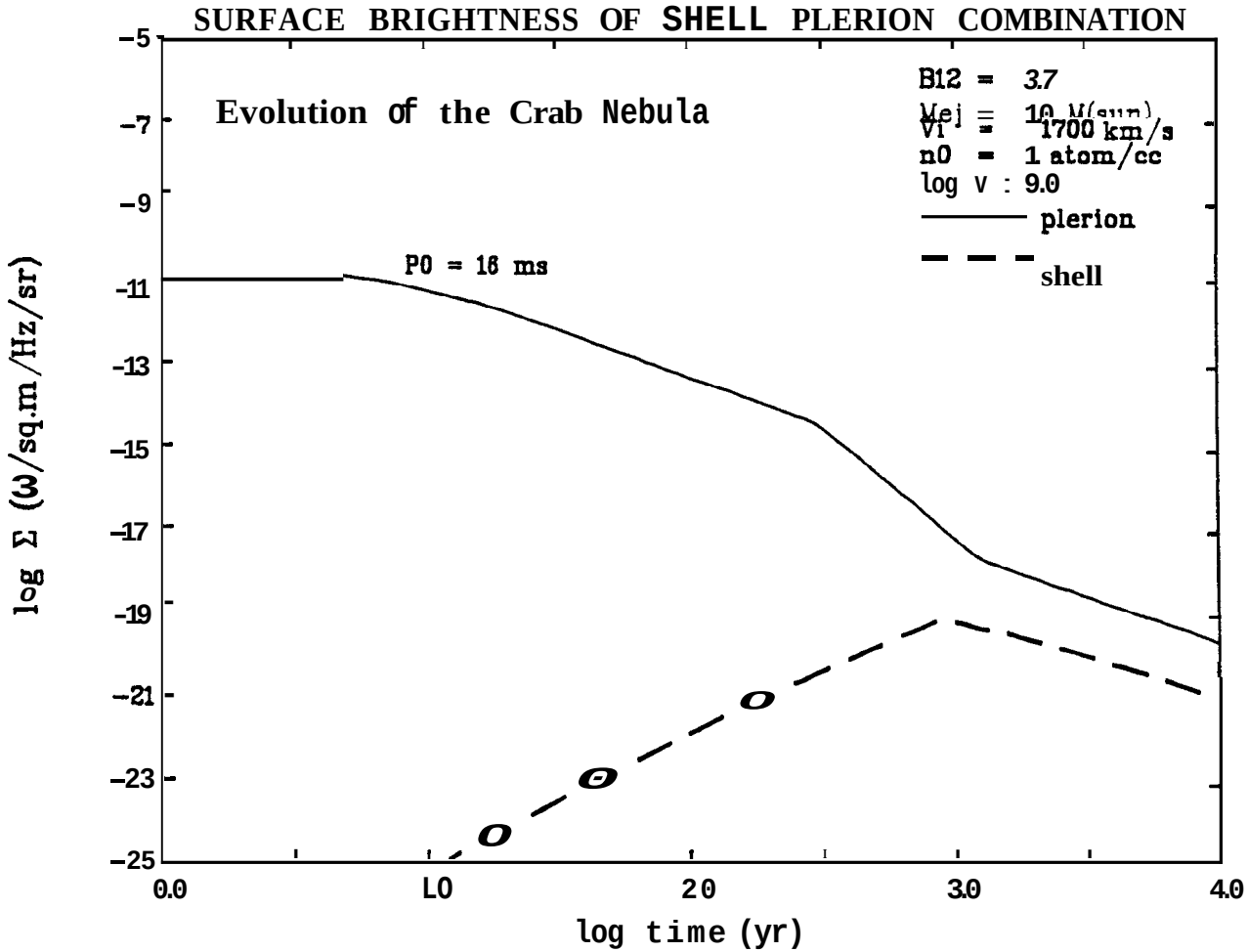

Fig. 5.3: Evolution of radio surface brightness of the shell and the plerionic components of the Crab nebula, assuming an ambient density of 1H atom/cc. The plerionic component is always much brighter than the shell and hence this remnant is not expected to evolve into a shell or a combination SNR.

shell (broken lines), for different values of the pulsar parameters and the velocity of expansion.

Fig. 5.3 shows the evolution of the Crab nebula. The initial velocity of expansion was assumed to be constant at 1700 km/s till deceleration sets in* . The mass in the ejecta was assumed to be 1 . It is interesting to note from fig. 5.3 that the shell component in this case will never be brighter than the plerion; the surface brightness of the plerion exceeds that of the shell by about two orders of magnitude. This clearly suggests that a plerionic remnant like the Crab nebula will, at no stage of its evolution, appear to have a shell, or a combination morphology. In fig. 5.3 we have assumed an ambient density of 1 atom/cc. A lower density will reduce the shell surface brightness further. The main reason for such a low luminosity of the shell is the low kinetic energy in Crab nebula's expansion ($\sim 10^{49}$ ergs as opposed to $\sim 10^{51}$ ergs in "standard" SNRs). Some authors (e.g. Chevalier 1977) have suggested that there may be a rapidly expanding shell at 3-4 times the present radius of the Crab nebula which carries most of the energy of the outburst. However, no observational evidence of such a shell exists. A reported detection (Murdin and Clark 1981) of an $H\alpha$ halo around the Crab nebula has not been confirmed. Very stringent upper limits have also been obtained on the radio emission (Velusamy 1985) and the X-ray emission (Mauche and Gorenstein 1985) from a possible fast shell around the

* Observations, in fact, show that there was an acceleration of the expansion as discussed in chapter 2.

Crab nebula.

Fig. 5.4 shows the evolution of a rapidly expanding ($V \sim 10000$ km/s) she11 remnant harboring different active pulsars. We have chosen the magnetic field of the pulsars to be equal to that of the Crab pulsar, but their initial spin periods to be 3, 16, and 100 ms respectively. The track corresponding to the 16 ms pulsar represents the nebula that would be produced by the Crab pulsar if placed inside a rapidly expanding cavity. We find from this figure that after the shell emission builds up, the average surface brightness of the shell region reaches almost the same level as the average surface brightness of the plerion. Both the shell and the plerion components will thus be clearly discernible, and the remnant will have a combination morphology with a rather strong plerion component*.

The plerionic nebula produced by a 3 ms pulsar in a rapidly expanding shell is very bright in the early phase, but by the time the shell emission has built up, the luminosity of the plerion has declined considerably, such that its resultant surface brightness is a factor of five below that of the shell. The reason for this is that in this case, though the

---

* The rather rapid decrease of the surface brightness of the shell region at times $\gtrsim$ 3000 years is caused by extrapolation of the polynomial relations (5.7) and (5.8) giving the magnetic field and the particle energy content in the shell region, and is therefore uncertain. The dotted line shows the evolution of the surface brightness assuming the energy content in field and particles to be independent of time after build up. When the shell grows to a large size, the compressed interstellar magnetic field behind the shock may also become important (van der Laan 1962), and change the above evolutionary picture.

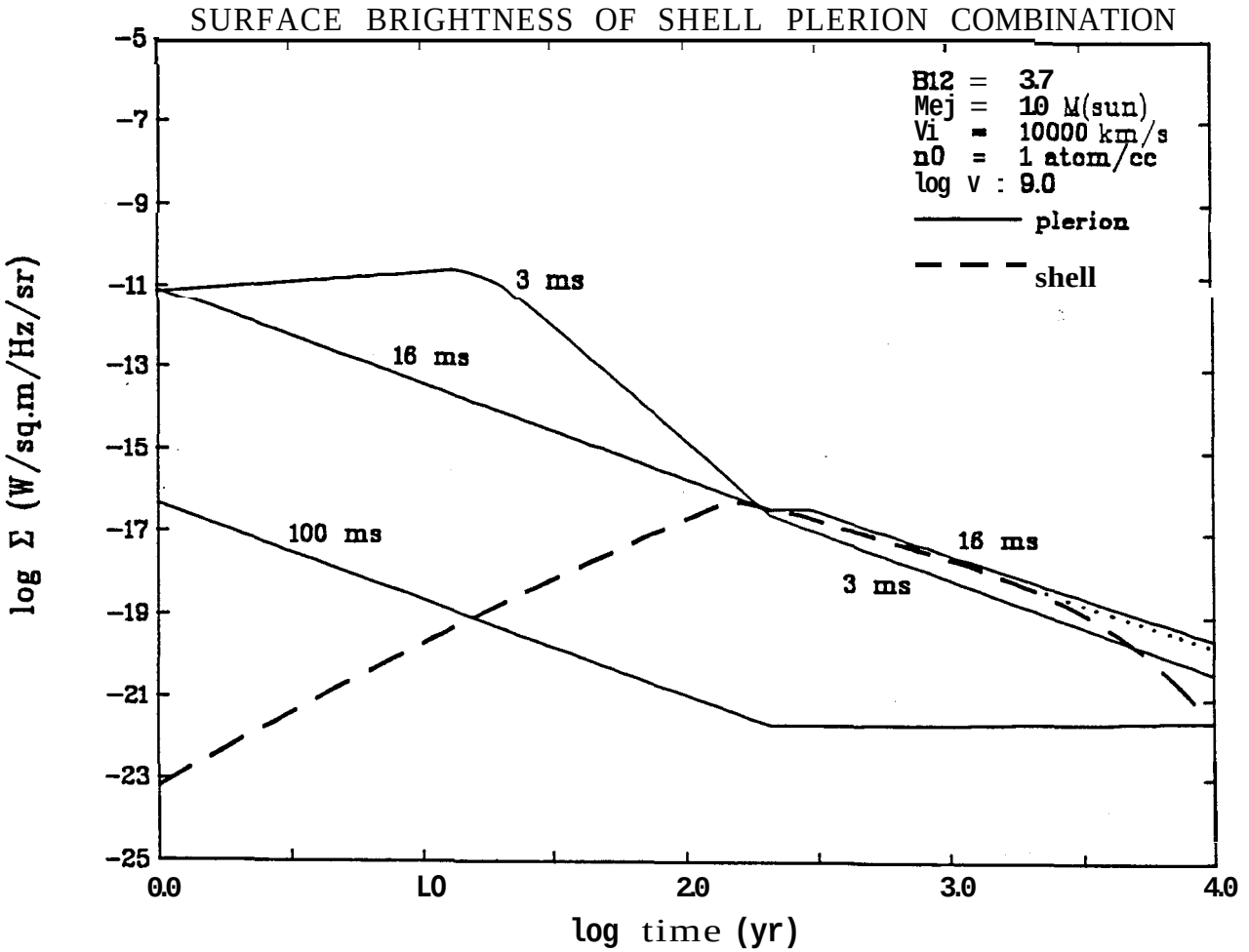

Fig. 5.4: The evolution of the surface brightness at 1 GHz of the plerionic and the shell components of a supernova remnant expanding in a uniform medium of density 1H atom/cc. Plerionic components produced by pulsars with initial rotation periods 3, 16, and 100ms are shown. 10^{12} B12 gauss is the magentic field assumed for these pulsars. Mej is the ejected mass, Vi the expansion velocity before deceleration, and n0 is the density of the ambient medium. The rapid decrease of shell surface brightness at times $>$ 3000 yr is an artifact of extrapolation of polynomial relations (5.7) and (5.8). The dotted line shows the evolution of the shell assuming the total energy in field and particles to be independent of time after build-up.

total energy released by the pulsar is large, most of this energy is deposited in the nebula in early stages when the size of the cavity is rather small. After that severe adiabatic losses reduce the energy content considerably. This remnant will look like a plerion for $\sim$100 years and will then have a combination morphology with a very weak plerionic component.

A $\sim$100 ms pulsar produces a plerionic nebula which is never very bright. For a brief period ($\sim$10 years) it does have a plerionic appearance (at this stage, however, it will be a point source for most radio telescopes) and later it evolves into a shell remnant. We thus see that both very slow and very fast pulaars would produce rather faint plerions which will not be easily distinguishable from the shell, whereas pulsars with an intermediate period will produce a brighter nebula. In the case of a very fast pulsar, the plerion luminosity decays too rapidly after the inital spindown timescale, $\tau_o \equiv P_o/2\dot{P}_o$. The nebulae produced by long-period pulsars never get very bright. The highest ratio of plerion-to-shell surface brightness is obtained when $\tau_o \approx t_o$, i.e. when the initial spindown timescale roughly equals the time when deceleration sets in. For a Crab-like pulsar, and the mass, velocity and ambient density chosen for the above models, this condition is very nearly satisfied.

While an expansion velocity of $\sim$10000 km s^{-1} may be appropriate for the ejecta in a typical Type I explosion, the expansion velocities in a typical Type II event are somewhat smaller. We have, therefore, also computed the evolution of plerions and shells for a smaller expansion velocity of $\sim$ 5000 km s^{-1}. To keep the blast energy $\sim 10^{51}$ ergs, we have increased the mass of the ejecta to $4M_{\odot}$ in this case. The results are presented in fig. 5.5, for pulsars with initial periods of 3, 16 and 100 ms respectively. The magnetic field is again chosen to be equal to that of the Crab pulsar, (3.7×10^{12} gauss). We find that the results are not qualitatively different. Here the deceleration sets in somewhat later, and as a result, the nebula produced by a Crab-like pulsar is weaker in the present case. The maximum plerion-to-shell brightness ratio will, in this case, be obtained for a pulsar with somewhat longer initial period than the Crab pulsar.

Two Stage Ejection

Reynolds and Chevalier (1984) have considered the evolution of supernova remnants where the ejection of matter takes place in two stages. A fast moving shell with $\sim$10-15 $M_{\odot}$ contains most of the blast energy. A few solar masses of material is left near the core, expanding with a very small velocity $\sim$300 km/s. The pulsar working at the centre creates a bubble of relativistic material around itself, and the pressure of this pulsar bubble eventually sweeps up this core

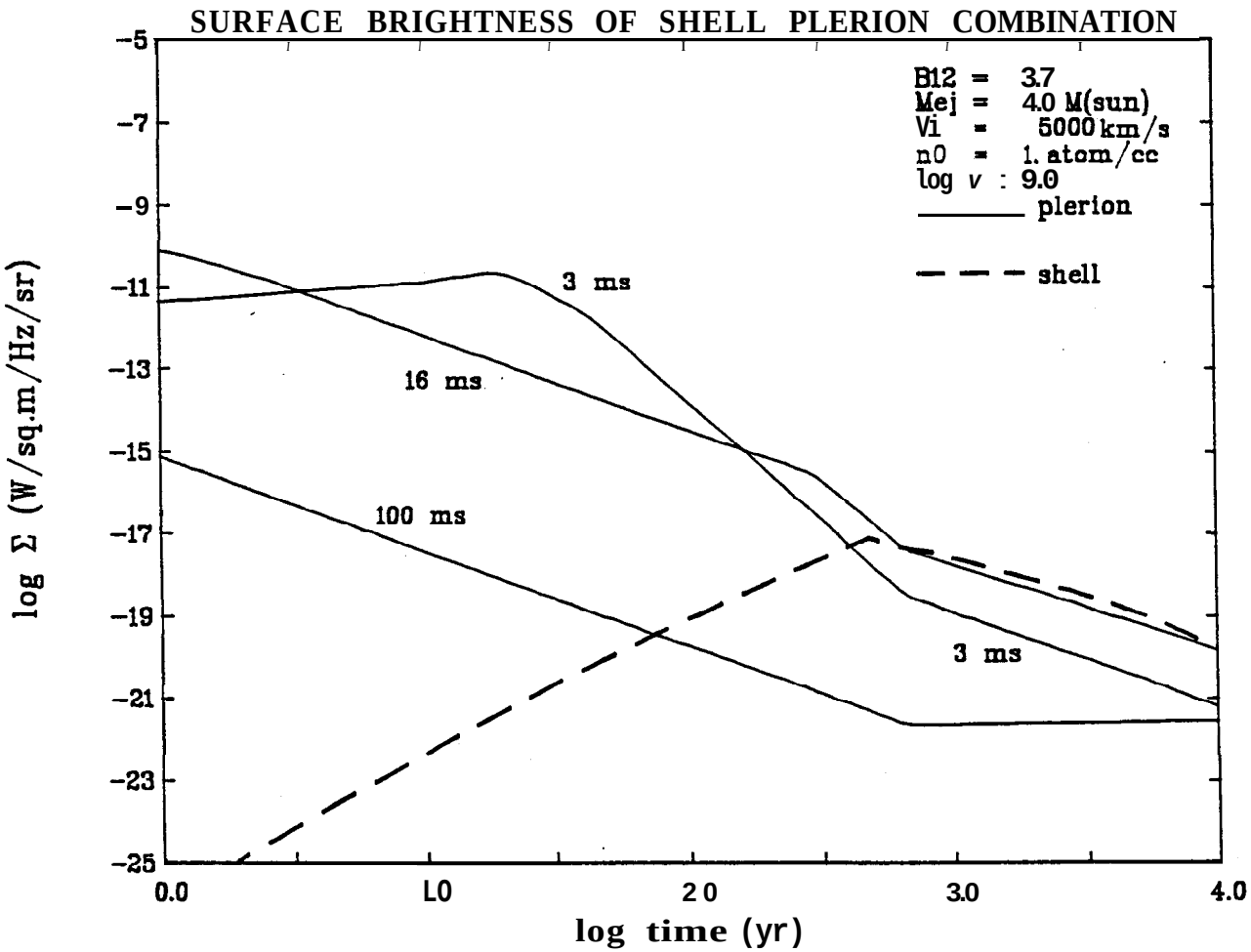

Fig. 5.5: Same as Fig. 5.4, with different values for Mej and Vi.

material and accelerates it, much in the same manner as described in apppendix 2.A1. The situation is sketched in fig. 5.6. The final expansion velocity attained by the core material, which also forms the boundary of the plerion, is usually much smaller than that of the outer shell. The fast outer shell will interact with the ambient medium and decelerate. The slowly expanding plerion at the interior, however, will not immediately feel this deceleration and will continue to expand freely. Some time later, the reverse shock will move in from the outer regions and compress the bubble, raising its luminosity and surface brightness. After this, the pulsar bubble will expand as $r \propto t^{0.3}$ and the outer shell as $r \propto t^{0.4}$. This picture is somewhat model dependent, the density distribution of the ejected matter being an important factor. Also, the details are difficult to treat analytically. We have, therefore, not attempted to compute the consequences of this model in detail. As explained above, in this model the expansion velocity of the plerion can be quite independent of that of the shell, and in this sense this model is somewhat less constrained than ours. Reynolds and Chevalier (1984) have presented the evolution of luminosity and surface brightness of several model remnants using this picture. The plerions in this case will be usually much brighter at a given time than those in the model we have considered. As a result, this'model will predict that most supernova remnants produced this way will have a shell-plerion combination morphology.

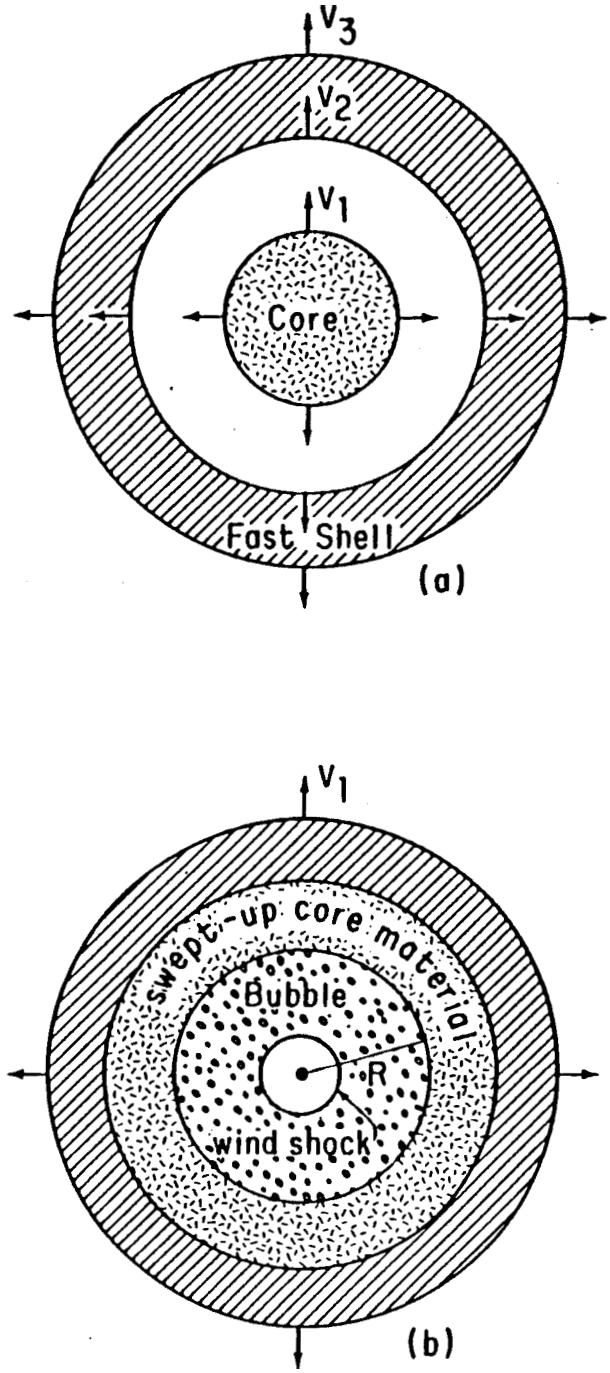

Fig. 5.6: Schematic representation of the structure of the supernova ejecta in the case of two-stage ejection. (a) An illustration of the Core-Shell model. The fast shell receives its kinetic energy from the initial blast wave. The slowly moving core material is later swept up by the pulsar bubble. (b) A larger view of the core. (from Reynolds and Chevalier 1984)

5.5 ROLE OF THE AMBIENT MEDIUM

5.5.1 Different Components Of The Interstellar Medium

In the previous section we have treated the interstellar matter as a uniform medium of density ~ 1 atom/cc. In reality, the interstellar medium is far more complex and consists of regions of different densities and temperatures co-existing in pressure equilibrium (Spitzer 1978). Small, dense clouds are immersed in a more diffuse, partially ionised substrate (fig. 5.7). Much of the information about the structure of the interstellar matter has emerged from the studies of the 21 cm line radiation of neutral hydrogen (e.g. Radhakrishnan et.al. 1972). The temperatures and densities of the small ($\sim$ a few pc) clouds were found to be $\lesssim$ 100 K and ~ 10 atom/cc respectively. The "warm" diffuse gas was found to have a temperature ~ 8000 K, and a density ~ 0.2 atom/cc. More recently, ultraviolet and X-ray observations of the interstellar medium have revealed the presence of a medium of much lower density and higher temperature ($T \sim 10^6$ K, $n \sim 3.10^{-3}$ atom/cc) (Rogerson et.al. 1973; Jenkins and Meloy 1974; York 1974; recent review in Cowie and Songaila 1986). This medium is referred to as the "coronal gas". The existence of this gas had in fact been predicted by Spitzer (1956) to explain the equilibrium of clouds at high galactic latitudes.

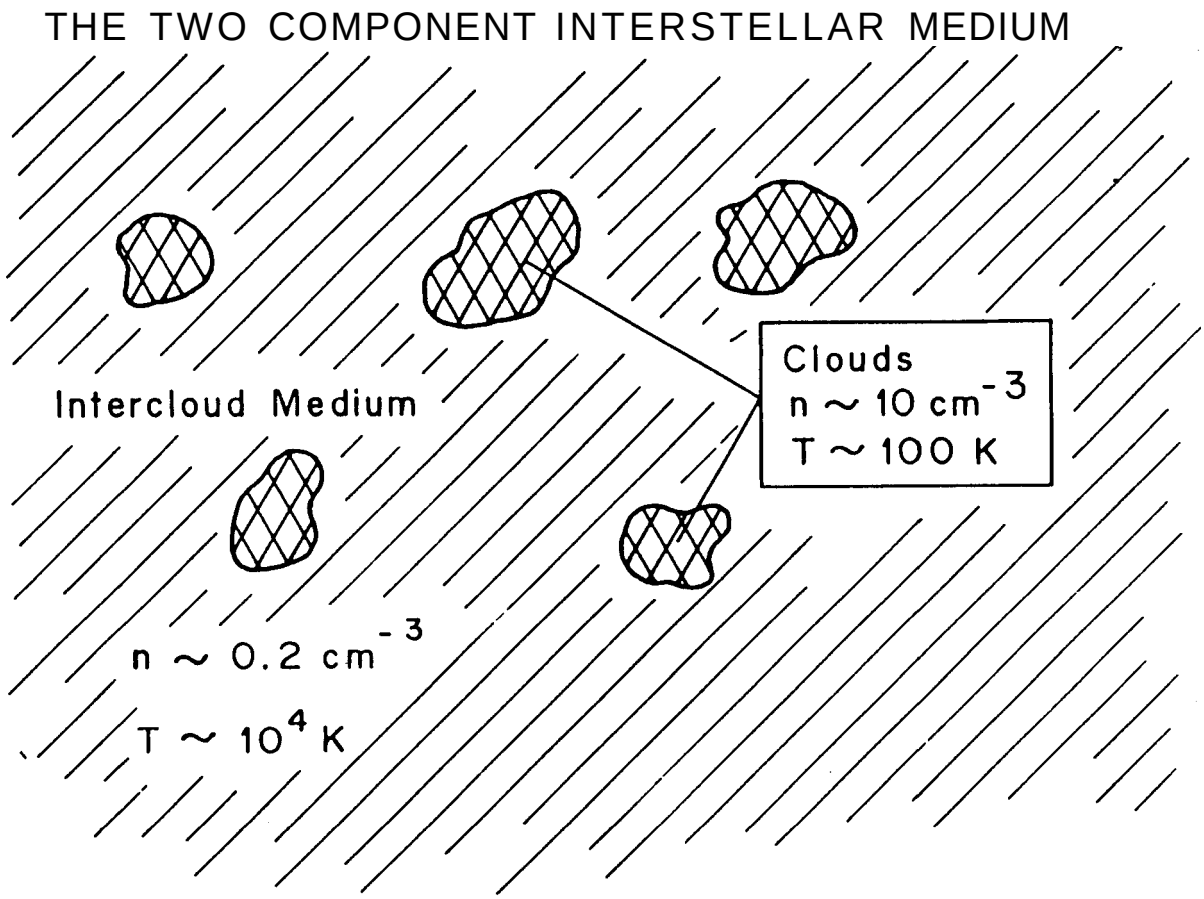
THE TWO COMPONENT INTERSTELLAR MEDIUM
Clouds
n ~ 10 cm^-3
T ~ 100 K
Intercloud Medium
n ~ 0.2 cm^-3
T ~ 10^4 K

Fig. 5.7

McKee and Ostriker have constructed a comprehensive and global picture of the interstellar medium in which the Coronal gas has a filling factor of $\sim$ 70%. The rest of the volume is occupied by clouds which now have an onion skin structure in which the innermost regions are cold and neutral with puffed up envelopes warm neutral and warm, partially ionized gas (see fig. 5.8) There is no room in their model for the conventional intercloud medium mentioned previously. But it is not clear what the true extent of the Coronal gas is; doubts have in fact been expressed about its global presence (see, e.g. Chevalier 1978; Heiles 1980).

Although a comprehensive model which is consistent with all observations is not yet available, it seems reasonable to suppose that in addition to the Coronal gas there must be regions in the Galaxy which are filled by warm ($T \sim 8000$ K) dense ($n_H \sim 0.2$ cm^{-3}) gas.

The question of how supernova remnants would evolve in the coronal gas is certainly an important one. The evolution of supernova remnants in a low density medium can be quite different from that in a uniform, dense medium - and this has been long recognized (e.g. Lozinskaya 1979; Higdon and Lingenfelter 1980; Srinivasan and Dwarakanath 1982). Shell remnants expanding in a low density medium will turn on later, and their peak luminosities will be smaller than those evolving in a dense medium. This reduces their lifetime, and changes their age and birthrate estimates. In addition, if such a remnant harbours an active pulsar, the evolution of its

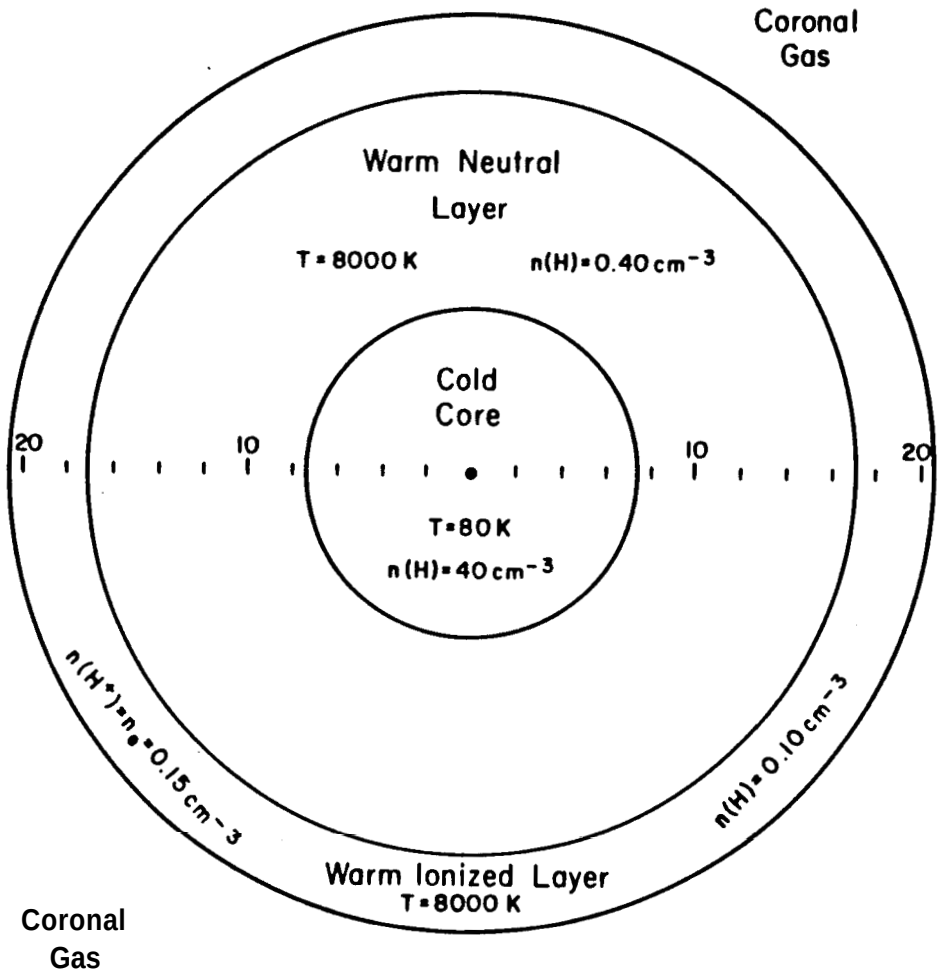

Fig. 5.8: The McKee-Ostriker model for the Interstellar Medium. A schematic view of a typical cloud, embedded in the Coronal gas, is shown. (Figure reproduced from Spitzer, 1982).

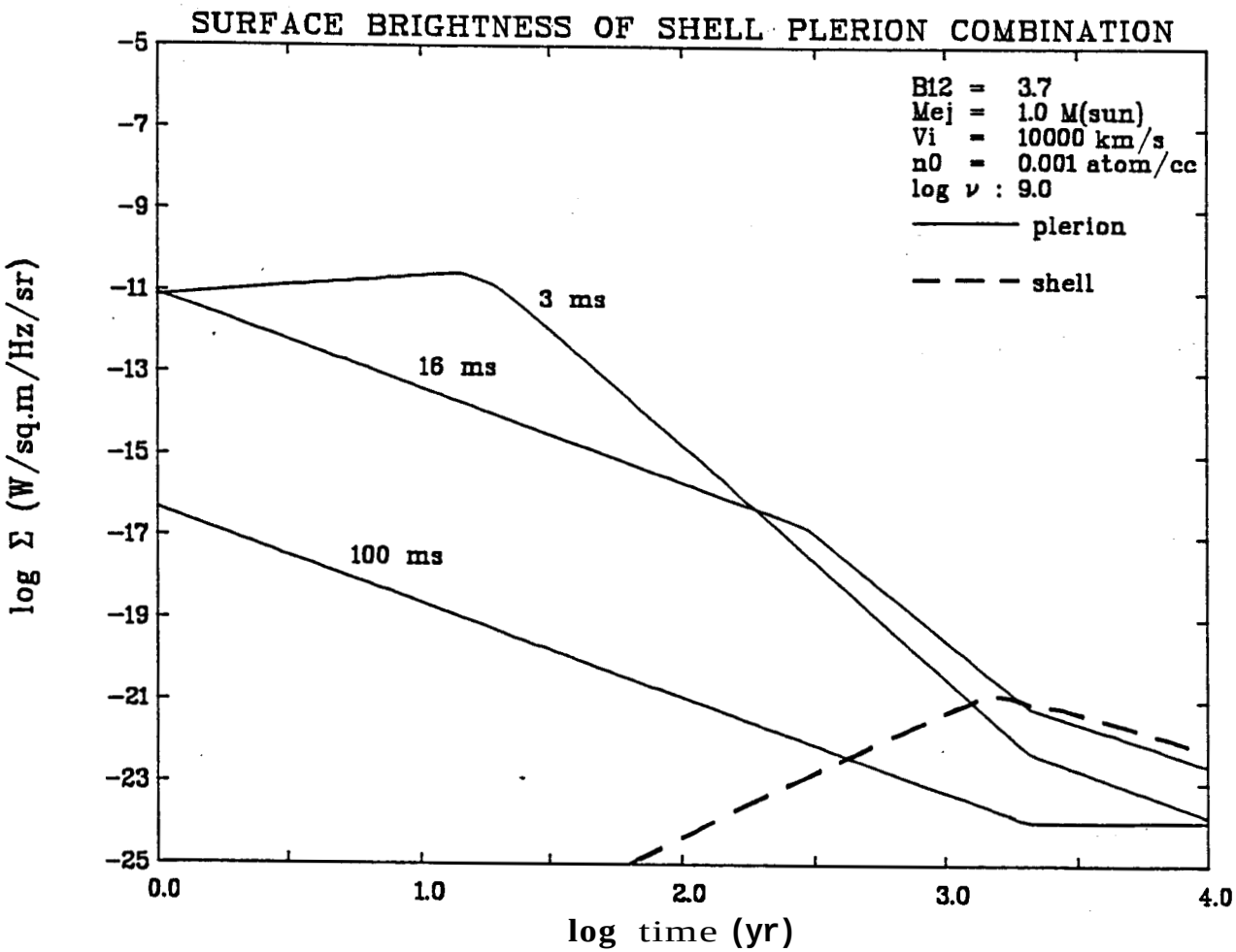

Fig. 5.9: The evolution of the plerionic and the shell components of supernova remnants expanding in the Coronal gas. See caption of Fig. 5.4 for explanation of symbols. Evolution of the plerionic component is shown for three different initial spin periods of the central pulsars.

morphology may also be quite different from that in a dense medium. We shall discuss this question below.

5.5.2 Evolution Of SNR Morphology In The Coronal Gas

To investigate the evolution of SNR morphology in different components of the ISM, we have computed the evolution of the surface brightness of the plerion and that of the shell component, with the external density set to $n \sim 10^{-3}$ atom/cc, a typical value for the Coronal gas. As in the previous section, we examined three cases in each set - initial rotation periods of 3 ms, 16 ms and 100 ms for the driving pulsars. The surface dipole field of the pulsars were assumed to be the same as that of the Crab pulsar, $\sim 3.7 \times 10^{12}$ gauss. The ejected mass and velocity of expansion were fixed at $1 M_{\odot}$ and 10000 km/s respectively. The results are shown in fig. 5.9. It is clear that as the density is reduced, the shell emission takes longer time to build up, and thus the nebula has a plerionic appearance for a longer time. Thus, in this case, more SNRs are likely to have a plerionic morphology than in the case of a denser medium.

5.6 DISCUSSION OF THE MORPHOLOGY OF SNR 0540-69.3

SNR 0540-69.3 in the Large Magellanic Cloud is one of the few known examples of pulsar-SNR associations. This remnant presents an interesting puzzle regarding its morphology. In X-ray, wavelengths it looks like a typical plerion; so much so that Clark et.al. (1982) predicted the presence of a pulsar in

it based on its X-ray appearance, and it was found. On the other hand, at radio frequencies, though the remnant is not fully resolved, its observed properties seem to suggest that it is a shell SNR. In this section we shall attempt to explain this apparent contradiction. Our suggestion is that the remnant is in fact a shell-plerion combination, with the **plerionic** component dominating in X-rays and the shell component producing most of the observed radio radiation.

The observed properties of this remnant are summarized in table 5.1. As is seen from the table, the resolution of the radio map available is not adequate to decide its morphology. Therefore let us first explain why we expect the radio remnant to be a shell. The first argument comes from its spectral index in radio and X-ray bands.

X-ray emission from young plerions is produced by high energy particles which lose energy predominantly by the Synchrotron process. On the other hand, the lower energy particles which produce radio emission lose energy primarily due to the expansion of the nebula. This latter kind of particles, when accumulated in the nebula, preserve the shape of the power law energy distribution with which they were injected:

$$N(E)dE \propto E^{-\gamma}dE .$$

But the energy exponent of the accumulated particle distribution steepens by 1 at higher energies, where the

Table 5.1 : The observed properties of SNR 0540-69.3

A. The SNR

Radio

843 MHz observation with the Molonglo Synthesis Telescope (HPBW = 43") indicates angular extent of ~ 30", i.e. a linear diameter ~8 pc (fig. 5.10) [1].

Flux at 843 MHz : 1.06 Jy [1].

Radio spectral index α_R : 0.43 ($I_\nu \propto \nu^{-\alpha_R}$) [1].

X-rays

Einstein Observatory HRI map clearly shows centrally condensed emission. Linear Diameter ~ 3 pc (fig. 5.11) [2].

Luminosity in 0.15-4.5 KeV band : ~ 10^{37} erg/s [2].
(25% of this comes from the pulsar [7]).

X-ray spectrum : power law with index α_X = 0.8 [3].

Optical

Strong [OIII] emission most pronounced in an annulus of ~ 2 pc in diameter (fig. 5.12). The [OIII] line shows velocity width ~ 2000-3000 km/s. An [OIII]-emitting filament ~ 5 pc away from the centre of this ring is also probably associated with the SNR [4].

Optical continuum has been detected from the Synchrotron Nebula (fig. 5.13) [5].

B. The Pulsar

PSR 0540-69.3 was first found in X-rays and later detected in optical [6,7,8].

Spin period P : 50 milliseconds [6,7].

Slowdown rate $\dot{P}$: 4.7×10^{-13} s s^{-1} [6,7].

The above values of P and $\dot{P}$ imply :

Surface magnetic field B_* ~ 4.9×10^{12} gauss, and

Spindown age t_{ch} ~ 1600 years.

References :

[1] Mills et. al. (1984)
[2] Mathewson et. al, (1983)
[3] Clark et. al. (1982)
[4] Mathewson et. al, (1980)
[5] Chanan, Helfand and Reynolds (1984)
[6] Seward, Harnden and Helfand (1984a)
[7] Seward, Harnden and Helfand (1984b)
[8] Middleditch and Pennypacker (1985)

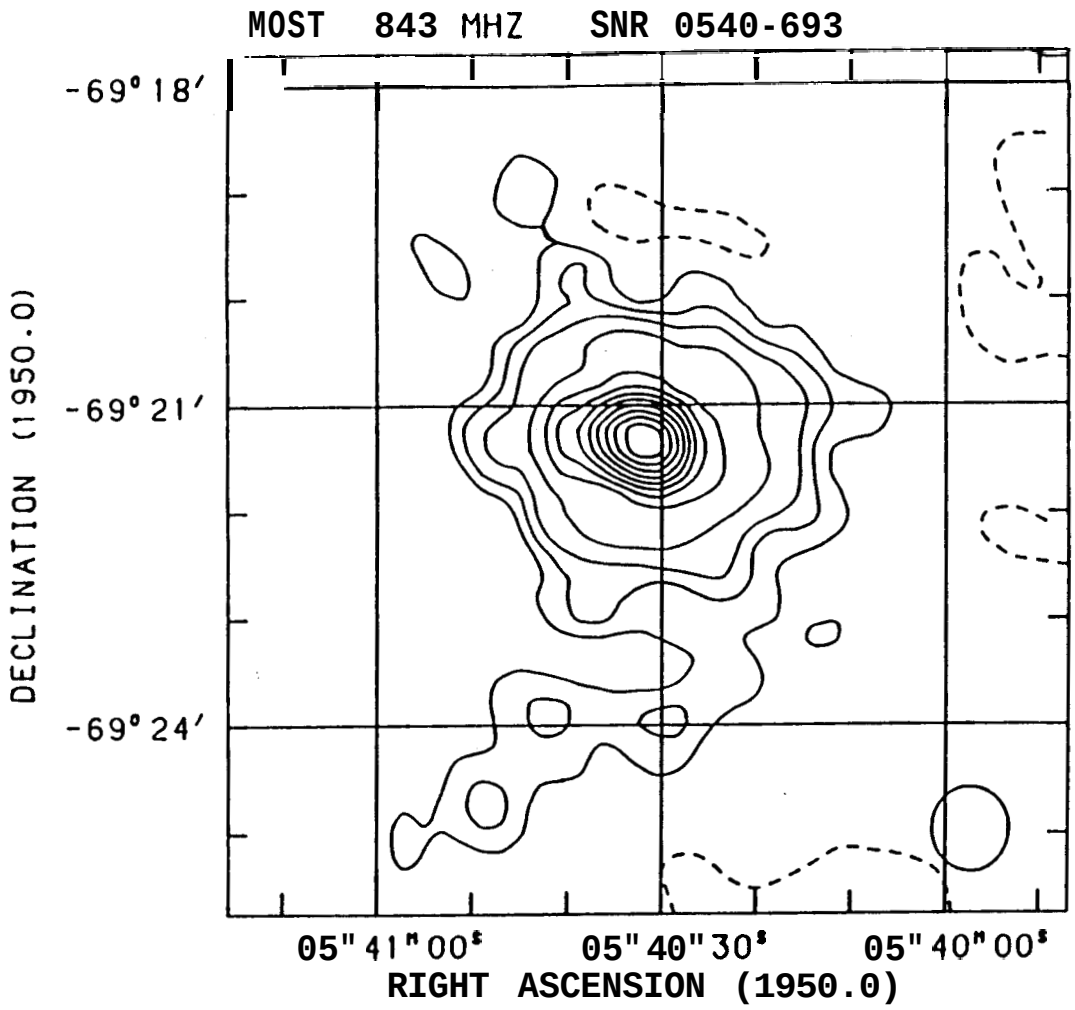

Fig. 5.10: A 843 MHz map of SNR 0540–69.3 obtained using the Molonglo Observatory Synthesis Telescope. While the central portion corresponds to the supernova remnant, the large extended emission around it may be related to the 30 Doradus region. FWHM beam is shown as an ellipse at the bottom right corner (Taken from Mills et. al. 1984).

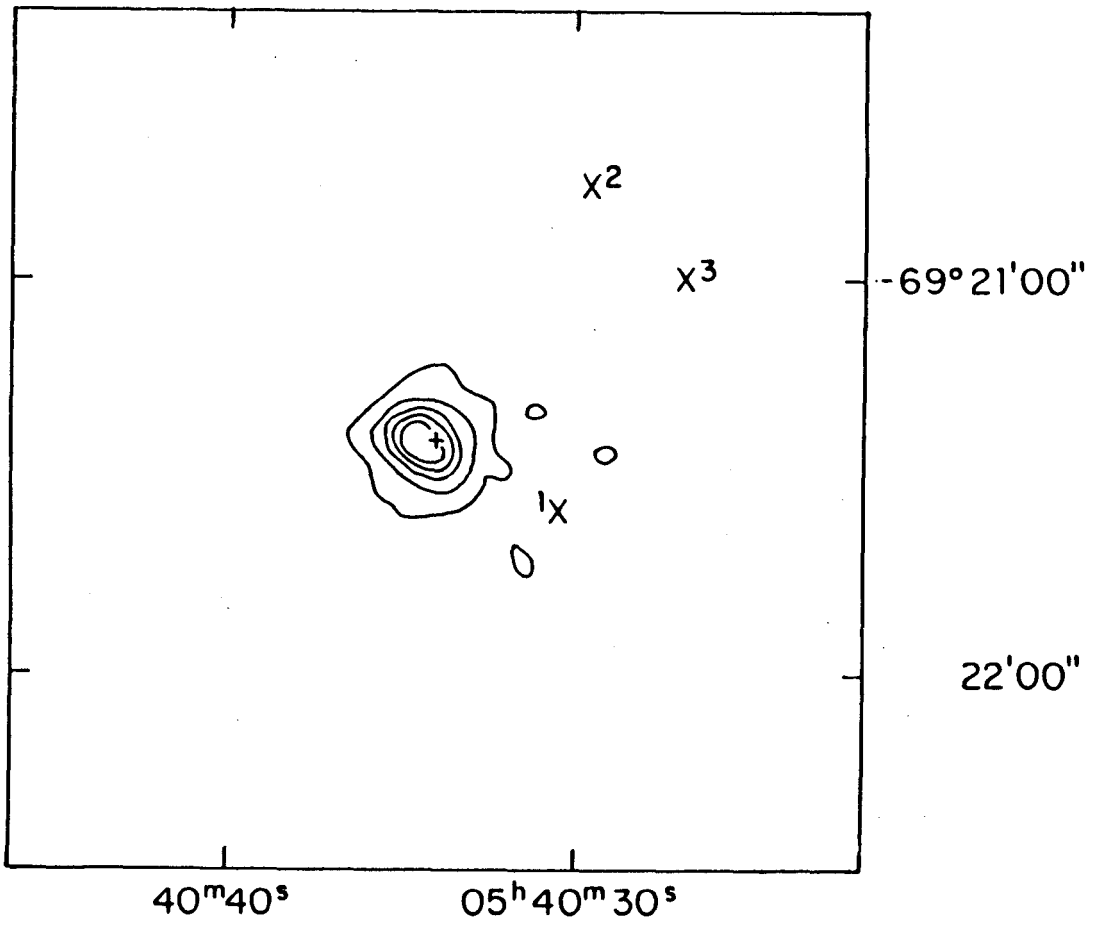

Fig. 5.11: X-ray map of SNR 0540-69.3 obtained using the HRI on board the Einstein Observatory by Mathewson et. al. (1983). Contour levels are 0.05, 0.25, 0.5, 0.75 and 1.0 counts s^{-1} $arcmin^{-2}$. Numbered crosses indicate the positions of reference stars. The plus sign (+) denotes the optical centre of the remnant.

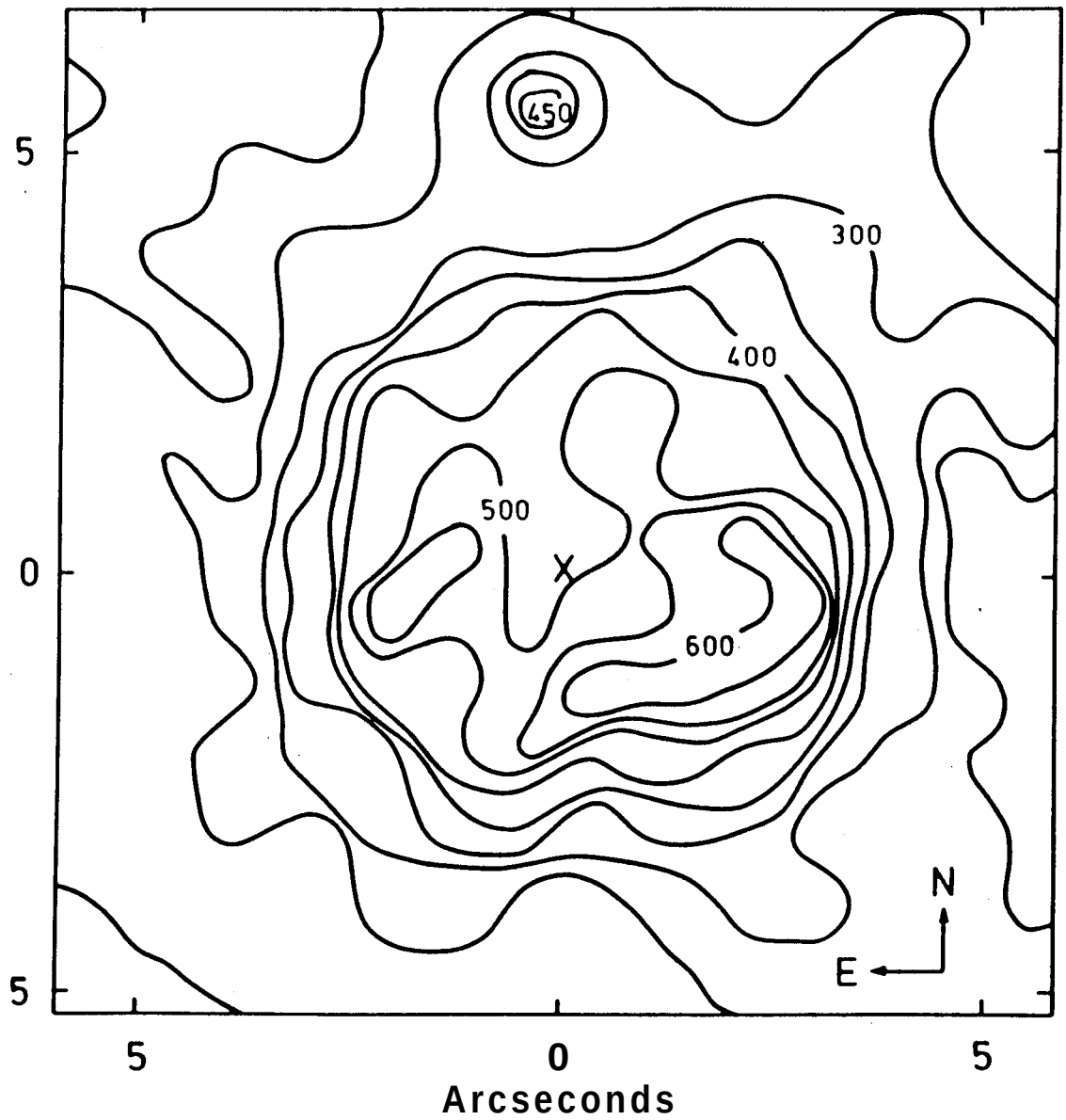

Contour map of the intense [O III] annulus, superposed on background nebulosity. Map center is at $\alpha = 05^h40^m35^s.2$, $\delta = -69°21'14''.3$, and the units are photons per pixel. The star at the north of the diagram indicates-the spatial resolution.

Fig. 5.12: Isophotes of [OIII] image of SNR 0540-69.3, clearly showing the annular emission region. (From Mathewson et. al. 1980).

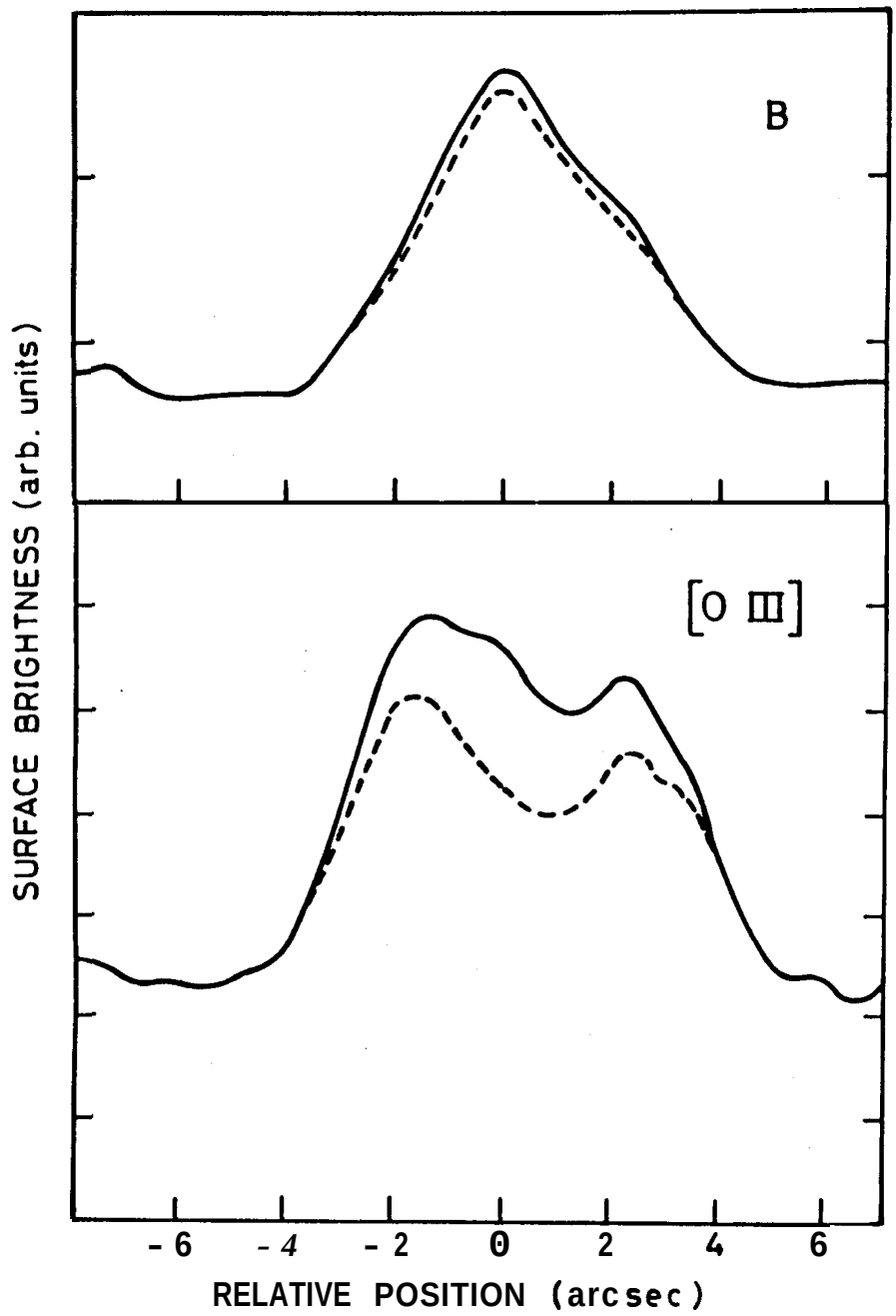

Fig. 5.13: East-West slices through the centre of the nebula 0540-69.3 in blue filter (top) and [OIII] filter (bottom). Dashed curves contain correction for unwanted contribution from line and continuum respectively. (From Chanan, Helfand and Reynolds, 1984).

energy loss is mainly due to radiation:

$$N(E)dE \propto E^{-(\gamma+1)}dE.$$

Thus the synchrotron radiation spectrum at lower frequencies is given by

$$I_\nu \propto \nu^{(1-\gamma)/2}$$

and that at higher frequencies by

$$I_\nu \propto \nu^{-\gamma/2}.$$

The X-ray spectral index α_X = 0.8 thus suggests that the spectrum of the injected particles must be of the form

$$N(E)dE \propto E^{-1.6}dE.$$

This would predict a radiation spectral index α_R=0.3 at radio wavelengths. The observed radio spectrum α_R= 0.43 is clearly much steeper than this, and fits in more closely with a standard shell supernova remnant. It should be remarked that in all known plerionic supernova remnants in the Galaxy, it appears that the injected spectrum of particles must have a "break", that is, the value of γ is somewhat larger at higher energies (Reynolds and Chanan 1984; Bhattacharya and Srinivasan, 1987; Srinivasan, 1985a; Davelaar et.al. 1986). For example, the Crab nebula has a radio spectral index α_R=0.3, which would imply an X-ray radiation index α_X = 0.8; but the observed X-ray emission has a spectral index α_X= 1.1.

If the same is true even for SNR 0540-69.3, then its radio spectrum would be expected to be even flatter than 0.3, making the inconsistency with observations even more glaring.

The second argument comes from the observed radio luminosity of the SNR. In an earlier work (Srinivasan and Bhattacharya, 1984) it was shown using simple scaling from the luminosity of the Crab nebula that the observed radio luminosity of SNR 0540 - 69.3 is much in excess of what one would expect from a plerion of its age and size, given the surface magnetic field of the energizing pulsar. Based on this conclusion, and the fact that the radio spectrum is much steeper than expected, it was suggested that this remnant must be a shell-plerion combination, with most of the radio flux coming from the shell component. We present here some refinements of this model.

A Model

The presence of a large amount of oxygen in this remnant suggests that its progenitor must have been a rather massive star. This, together with the rather small expansion velocity, indicates a substantial mass in the ejecta, assuming a standard explosion energy $\sim 10^{51}$ erg. We assume the mass in the ejecta to be $M_{ej} \sim 10\ M_\odot$ and an ambient density $n_o \sim 1$ atom/cc. The original expansion velocity is taken to be ~ 3500 km/s. Given these parameters, and the pulsar field $\sim 4.9 \times 10^{12}$ G, the X-ray luminosity of the plerion is best fit by an initial period $\sim$ 20 millisecond, which implies an age

$\sim$1400 yr for the remnant. The evolution of spectral luminosity at 4 KeV is sketched in fig. 5.14(a). The point marked "+" gives the observed X-ray luminosity of SNR 0540-69.3.

Using this initial spin period of the pulsar, and the other parameters mentioned above, we can now compute the evolution of radio surface brightness of both the plerion and the shell components, following the method used in the previous section. The result is shown in fig. 5.14(b). We find that the shell component accounts for most of the emission, the plerion contributing less than $\sim$ 25%. The observed average surface brightness, $\sim 5 \times 10^{-19}$ W/m^2/Hz/sr at 1 GHz, shown by the "+" mark, is quite consistent with the expected value.

A natural question that would arise at this point is that if the unresolved shell remnant contributes most of the radio flux, why doesn't it show up in the X-ray map? The HRI should certainly have been able to resolve it. This question can be answered using the X-ray Σ -D relation for LMC SNRs given by Mathewson et.al. (1983). For a shell of diameter $\sim$8 pc one expects a surface brightness $\Sigma_X \sim 10^{-3}$ erg cm^{-2} s^{-1}sr^{-1}, while the observed centrally condensed X-ray nebula has an average surface brightness $\Sigma_X \sim 0.12$ erg cm^{-2} s^{-1}sr^{-1}. The lowest contour presented by Mathewson et.al. (1983) in the HRI map of this remnant corresponds to $\sim 10^{-2}$ erg cm^{-2} s^{-1}sr^{-1}, about an order of magnitude larger than the expected X-ray brightness of the shell. Thus one does not expect the X-rays from the

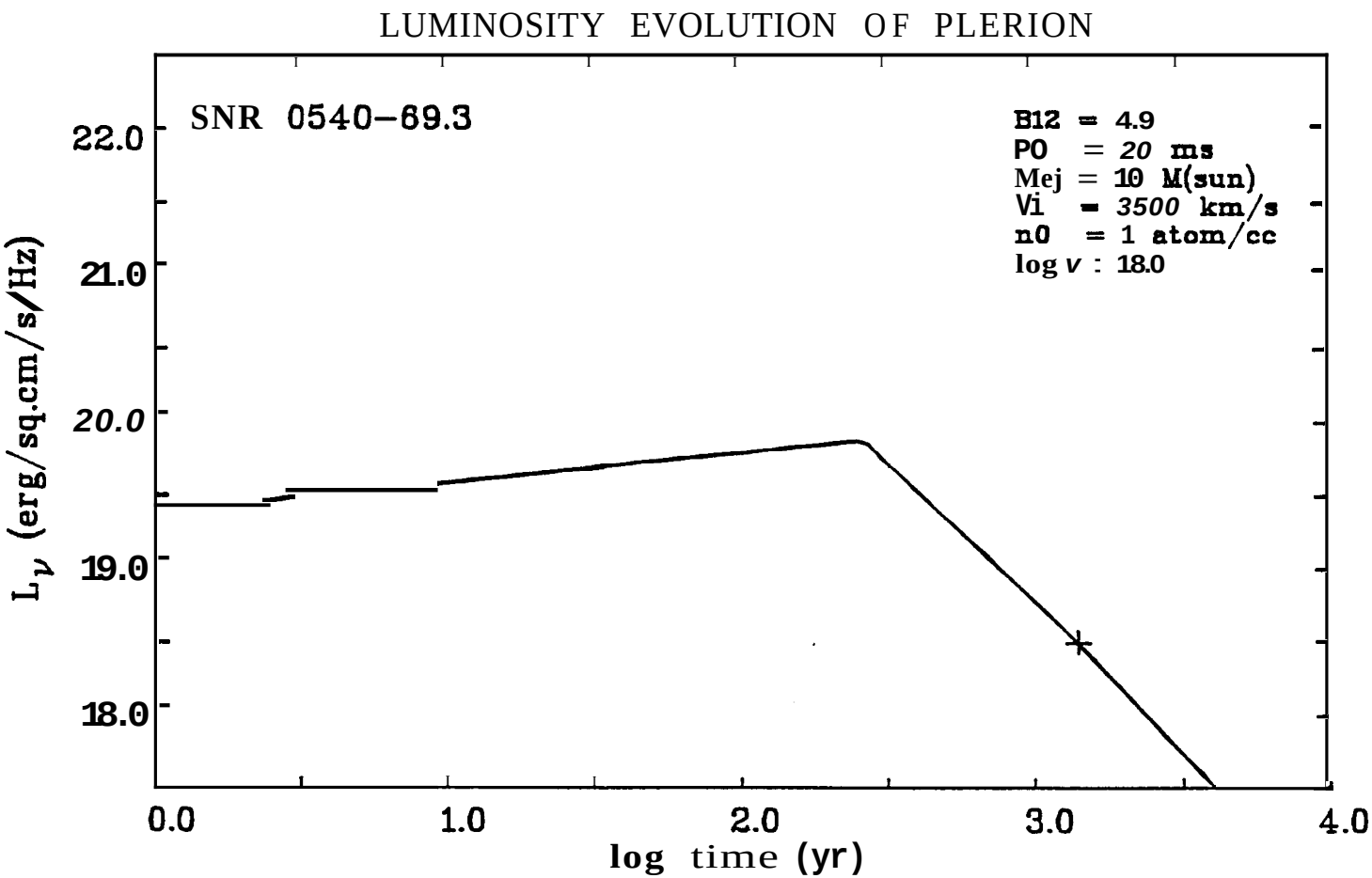

Fig. 5.14 (a): A model evolution of the X-ray luminosity of the plerionic component of SNR 0540-69.3. The '+' sign marks the observed value.

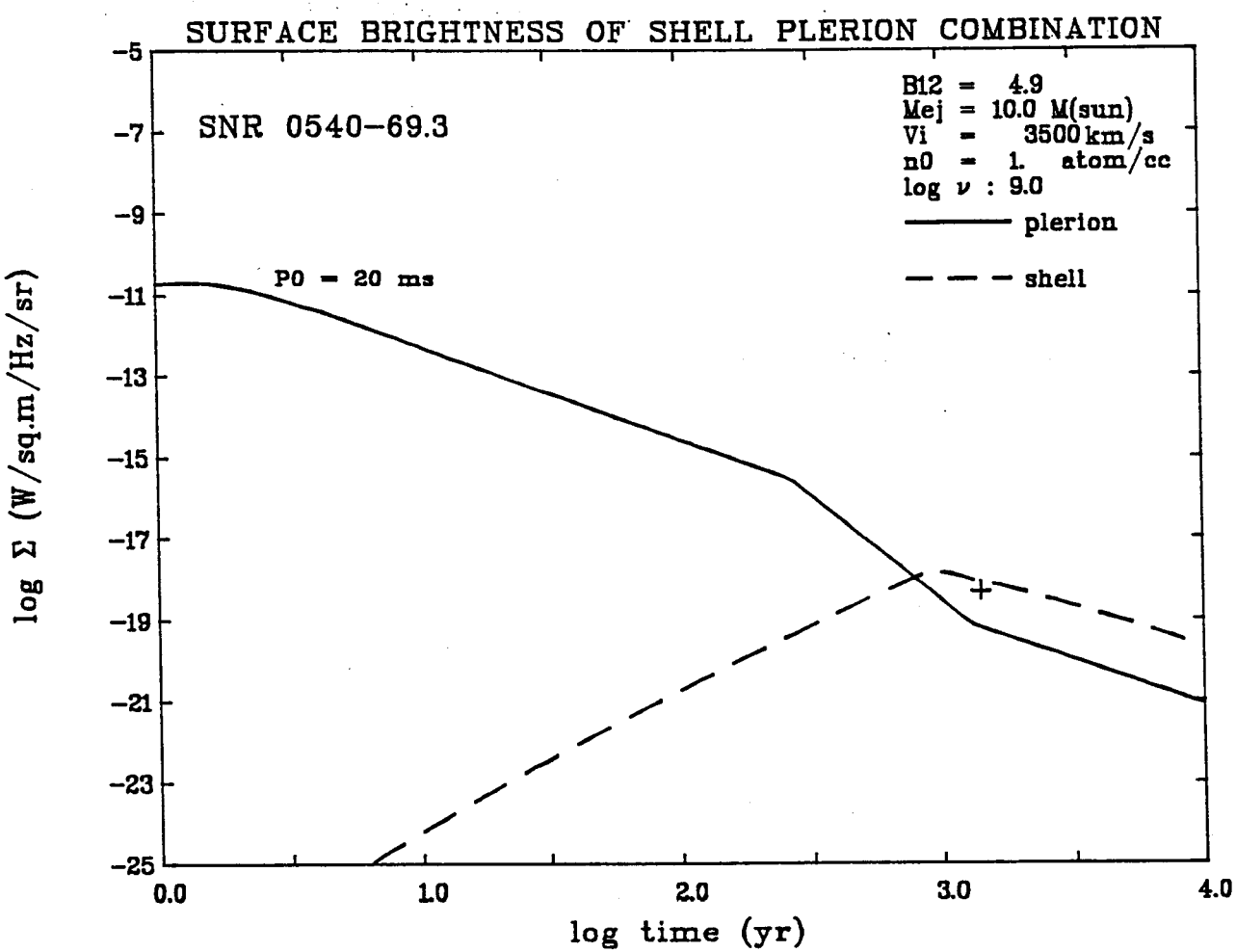

Fig. 5.14 (b) A model evolution of the radio surface brightness of the shell and the plerion components of SNR 0540-69.3. The observed value is indicated by the '+' mark.

radio-emitting shell to show up in the HRI map.

Another interesting feature of this remnant is the ring of [OIII] emission around the pulsar. The optical synchrotron nebula discovered by Chanan, Helfand and Reynolds is contained within this (fig. 5.13). It is thus tempting to suggest that this, in fact, is the boundary of the plerion. Reynolds (1985) has presented a model based on this picture. However, the fact that the observed X-ray nebula is twice as big as the [OIII] annulus cannot be accommodated in this model. There may be a low-brightness extension of the optical nebula beyond the annulus, which may be difficult to detect because of the presence of complex background nebulosity connected to the 30 Doradus region. We therefore suggest the following alternative picture. It is quite conceivable that a significant fraction of the ejected mass broke up into filaments, presumably due to a Rayleigh-Taylor instability triggered by the pressure of the pulsar bubble. Such filaments may be expected to be found at all distances from the pulsar as in the Crab nebula. The [OIII] annulus may then correspond to some enhanced excitation at that radius, for example by a standing shock located there. The existence of such a standing shock inside the Crab nebula was suggested by Rees and Gunn (1974). This shock corresponds to the radius where the directed (ram) pressure of the relativistic wind from the pulsar equals the built up ambient pressure inside the bubble. The pressure inside the bubble comes mainly from the built up magnetic field, since the energy density in

particles is reduced substantially due to radiation losses. The energy density in the magnetic field can be roughly estimated as follows:

The pulsar releases half of its stored rotational energy E_o over the first characteristic age τ_o. After τ_o the rate of energy release falls rapidly, and the evolution of the field energy is determined roughly by conservation of magnetic flux after $t = \tau_o$, which corresponds to pure adiabatic loss of field energy. If one assumes that $\sim$ 50% of the injected energy goes into the magnetic field, then the total magnetic energy at a time $t > \tau_o$ is

$$W_B(t) \simeq \frac{1}{8} E_o \cdot \frac{R_{neb}(\tau_o)}{R_{neb}(t)}$$

where R_{neb} is the nebular radius.

The factor $\frac{1}{8}$ comes from the fact that $\frac{1}{2} E_o$ is the total energy released by the pulsar upto τ_o, half of that is injected in the form of magnetic field, and half of the total injected field energy goes into adiabatic losses upto $t = \tau_o$. The second factor $R_{neb}(\tau_o)/R_{neb}(t)$ takes into account adiabatic losses occurring after $t = \tau_o$. The pressure due to the magnetic field would be then

$$p_{mag} = \frac{1}{3} \frac{W_B}{\frac{4\pi}{3} R_{neb}^3(t)} \; a \; \frac{1}{32\pi} \frac{E_o R_{neb}(\tau_o)}{R_{neb}^4(t)} .$$

This should balance the ram pressure of the pulsar wind at the shock radius R_s:

$$p_{ram} = \frac{L_{PSR}(t)}{4\pi R_s^2 c} = p_{mag} = \frac{1}{32\pi} \frac{E_o R_{neb}(\tau_o)}{R_{neb}^4(t)}$$

$$R_s \simeq \left[\frac{8 L_{PSR}(t)}{c E_o R_{neb}(\tau_o)}\right]^{1/2} R_{neb}^2(t). \qquad (5.10)$$

Using an initial spin period $P_o \sim 20$ ms for the pulsar, an initial expansion velocity ~ 3500 km/s for the nebula and the present observed parameters of the pulsar and the nebula, we obtain $R_s \sim 0.8$ pc from the above expression. This is remarkably close to the radius of the observed [OIII] ring. Thus the size of the annulus is fully consistent with the presence of an enhanced excitation at R_s. This feature must in fact be filamentary, otherwise the relativistic particles could not have propagated beyond it. An optical image at higher resolution, with for example the Hubble Space Telescope, may be able to verify this. The large velocities upto $\sim$ 1500 km s^{-1} are probably caused by these filaments being strongly accelerated by the pulsar wind. One would naturally ask if there is a similar feature in the Crab nebula. From the published pictures of the Crab nebula it is not possible to discern any such feature. It appears that there is very little thermal matter near the shock region (which is identified to be the region of wisp activity by Rees and Gunn 1974), and as a result no ring-like emission is seen.

We see, therefore, that the above model for SNR 0540 - 69.3, comprising of a shell-plerion combination remnant with an inner shock, can successfully accommodate all observed features. It is interesting that the best estimate of the initial rotation period of the pulsar turns out to be $\sim$ 20 ms,

very close to that of the Crab pulsar. The magnetic field of this pulsar, too, is very close to that of the Crab pulsar. This lends support to the conclusion arrived at Chapter 2 - that

> long-lived and bright plerions are expected only in those circumstances where the central pulsar has an initial period $\sim$ 10-20 milliseconds and a magnetic field $\sim 10^{12.5}$ gauss, and the ejecta expand relatively slowly.

5.7 CONCLUSION

In an attempt to understand the evolution of SNR morphology, we have studied in this chapter the evolution of both the shell and the plerion components of supernova remnants. Based on a very simple model in which these two components of the SNR evolve essentially independently, but share a common velocity of expansion, we are able to identify cases where the remnant would appear to have a shell, a plerion, or a combination morphology. It is interesting to note that pulsars very similar to the Crab pulsar in initial period and magnetic field produce the brightest plerions which maintain their identity for a long time. In particular, the Crab nebula with its small expansion velocity is never going to build up a prominent shell. A remnant containing a pulsar with either too fast or too slow initial rotation has a plerionic appearance at first, but at a later stage evolves into a shell remnant. These results can be summarized in a

tabular form as follows:

Pulsar's initial spin	Strong Explosion	Weak explosion
Fast	Bright Plerion => Shell	"Pulsar-driven" remnant Bright Plerion => Shell
Medium	Bright Plerion => Combination	Bright Plerion
Slow	Weak Plerion => Shell	Weak Plerion => Combination

The pulsars in the above table are assumed to have magnetic field similar to that of the Crab pulsar. "Fast" corresponds to $P_o \sim 3$ ms, "Medium" to $P_o \sim 20$ ms and "Slow" to $P_o \sim 100$ ms. A "strong" explosion stands for a standard supernova outburst with $\sim 10^{51}$ ergs of blast energy. A "weak" explosion assumes a blast energy of $\sim 10^{49}$ ergs, similar to that of SN 1054.

This simple model of evolution is also able to account for all observed features of the supernova remnant 0540-69.3 in the Large Magellanic Cloud in which a pulsar has recently been found. Application of this model also leads to an estimate of the initial spin period of the pulsar contained in this remnant. We find an initial period $P_o \sim 20$ ms for the pulsar 0540-69.3.

As already mentioned, the model considered above is a very simple one. It will certainly be worthwhile to investigate this problem with a more refined model, incorporating the detailed dynamics of the shock front, and of the interface between the pulsar bubble and the ejected matter. One should also allow for mixing of relativistic particles from the pulsar bubble with the ejecta, which may modify the way the shell luminosity behaves with time. Rayleigh-Taylor instabilities at the plerion-ejecta interface and the formation of filaments may also be important. Such an effort, however, is outside the scope of this thesis and will be attempted elsewhere.

APPENDIX 5.A1

MAGNETIC FIELD AND PARTICLE DISTRIBUTION IN A PLERION IN DECELERATED EXPANSION

In this appendix we derive the magnetic field and particle distribution in a plerion which after an initial phase of uniform expansion, is undergoing deceleration due to interaction with the ambient matter.

The nebula is assumed to expand with a constant velocity v upto a time $t = t_0$, following which the radius of the nebula increases as

$$R = v t_0 \left(t/t_0\right)^{\eta}, \quad \eta < 1. \qquad (5.A1.1)$$

The evolution magnetic field and particle content of the nebula during the free expansion phase has been discussed in appendix 2.A2. In this appendix we shall discuss the evolution beyond $t = t_0$.

We shall consider two distinct cases. In case A the deceleration occurs in phase II, i.e., $t_0 < \tau_0$, the initial characteristic slowing down timescale of the pulsar powering the nebula. In case B the nebula decelerates in phase III, i.e., after the initial spindown timescale of the pulsar $(t_0 > \tau_0)$.

As in appendix **2.A2,** we approximate the evolution of the pulsar's **spindown** luminosity as

$$L_{PSR}(t) = L_o \quad \text{for } t < \tau_o$$

$$\text{and} \qquad L_{PSR}(t) = L_o \left(\frac{t}{\tau_o}\right)^{-\alpha} \quad \text{for } t > \tau_o$$

and we follow the method outlined in appendix. **2.A2** to determine the nebular magnetic field and particle distribution.

Case A

In this case deceleration occurs before $t = \tau_o$, and hence both phase II and phase III are modified.

Phase II

At $t_o < t < \tau_o$, the magnetic field is obtained using **(2.A2.5)** and **(5.A1.1):**

$$B(t) = \left(\frac{6\epsilon_m}{1+\eta} \cdot \frac{L_o}{v^3}\right)^{1/2} t_o^{\frac{3}{2}(\eta-1)} t^{(1-3\eta)/2} \qquad \textbf{(5.A1.2)}$$

where ϵ_m is the fraction of the pulsar's **spindown** luminosity going into the magnetic field.

The break energy E_b, above which the particles lose energy mainly by radiation is given by

$$E_b = \frac{1}{c_1 B^2 (R/\dot{R})} = \frac{\eta(1+\eta)}{6\epsilon_m c_1} \cdot \frac{v^3}{L_0} \cdot t_0^{3(1-\eta)} \cdot t^{3\eta-2} \cdot$$

.....(5.A1.3)

At energies $E < E_b$, there will be two kinds of particles, (a) the relic particles injected before $t = t_0$, and (b) the fresh particles injected after $t = t_0$. It can be shown that the fresh particles make the dominant contribution. For them,

$$E_i = E \left(t/t_i\right)^{\eta}$$

and $$\frac{\partial t_i}{\partial E} = \frac{t}{\eta} \frac{E^{\frac{1}{\eta}-1}}{E_i^{1/\eta}} \quad .$$

E_i, t_i are defined through the relation that a particle injected with energy E_i at time t_i arrives at energy E at time t.

The energy distribution of particles in this energy range is then obtained from (2.A2.15):

$$N(E,t) = \frac{(2-\gamma)\epsilon_p L_0 E_{max}^{\gamma-2}}{1+\gamma-\eta} \cdot t \cdot E^{-\gamma} \qquad (E < E_b) \qquad (5.A1.4)$$

where ϵ_p is the fraction of the pulsar's spindown luminosity going into relativistic particles; γ and

E_{max} are the power law exponent and the maximum energy of the particle distribution respectively.

At energies $E > E_b$

$$\frac{1}{E} - \frac{1}{E_i} = \frac{6\epsilon_m C_1}{(1+\eta)(2-3\eta)} \frac{L_0}{V_3} t_0^{3(\eta-1)} \left[t^{2-3\eta} - t_i^{2-3\eta} \right]$$

which yields $t \simeq t_i$, and

$$\frac{\partial t_i}{\partial E} \simeq \frac{(1+\eta) v^3}{6\epsilon_m C_1 L_0} \cdot t_0^{3(1-\eta)} \cdot \frac{t^{3\eta-1}}{E^2} .$$

Hence

$$N(E,t) = \frac{(1+\eta)(2-\eta)\epsilon_b}{6(\eta-1)\epsilon_m C_1} E_{max}^{\eta-2} v^3 t_0^{3(1-\eta)} t^{3\eta-1} \times E^{-(\eta+1)} \quad (E > E_b) \qquad \ldots\ldots(5.A1.5)$$

Phase III

At $t > \tau_0 > t_0$, the magnetic field is given by

$$B(t) = \left[\frac{6\alpha\epsilon_m}{(1+\eta)(\alpha-\eta-1)} \cdot \frac{L_0}{v^3} \right]^{1/2} t_0^{\frac{3}{2}(\eta-1)} \tau_0^{(1+\eta)/2} t^{-2\eta} .$$

$\ldots\ldots(5.A1.6)$

The break energy is

$$E_b = \frac{\eta(1+\eta)(\alpha-\eta-1)}{6\alpha\epsilon_m c_1}\,\frac{v^3}{L_0}\,t_0^{3(1-\eta)}\,\tau_0^{-(1+\eta)}\,t^{4\eta}.$$

.....(5.A1.7)

At $E>E_b$, synchrotron losses dominate, and

$$t\simeq t_i\;;\;\frac{\partial t_i}{\partial E}\simeq\frac{(1+\eta)(\alpha-\eta-1)}{6\alpha\epsilon_m c_1}\cdot\frac{v^3}{L_0}\cdot t_0^{-3(\eta-1)}\tau_0^{-(1+\eta)}\cdot\frac{t^{4\eta}}{E^2}.$$

.....(5.A1.8)

Hence

$$N(E,t)=\frac{(2-\gamma)\epsilon_b}{(\gamma-1)\epsilon_m}\cdot\frac{(1+\eta)(\alpha-\eta-1)}{6\alpha c_1}\cdot E_{max}^{\gamma-2}\,v^3\,t_0^{3(1-\eta)}$$
$$\times\tau_0^{\alpha-\eta-1}\,t^{4\eta-\alpha}\,E^{-(\gamma+1)}$$
$$(E>E_b).$$

.....(5.A1.9)

The relic particles of phase II are found mainly below the energy $E_c\equiv E_b(\tau_0)\,(t/\tau_0)^{-\eta}$. At $E<E_c$ both the relic particles and the fresh particles make a comparable contribution. The energy distribution works out to be

$$N(E,t) = \frac{\{\alpha + \eta(1-\eta)\}(2-\eta)}{(1+\eta-\eta)(\alpha-1-\eta\eta+\eta)} \epsilon_p L_0 E_{max}^{\eta-2} \tau_0^{1+\eta(\eta-1)} \times t^{\eta(1-\eta)} E^{-\eta}$$

$$(E<E_c).$$

.....(5.A1.10)

Between E_c and E_b the spectrum is dominated by fresh particles which undergo only adiabatic losses. The particle energy distribution in this interval is given by

$$N(E,t) = \frac{(2-\eta)\epsilon_p E_{max}^{\eta-2} L_0}{(\alpha-1)-\eta(\eta-1)} \left[\frac{\eta(1+\eta)(\alpha-\eta-1)\beta^3}{6\alpha\epsilon_m C_1 L_0}\right]^{\frac{\alpha+\eta-1-\eta\eta}{5\eta-1}} \times \tau_0^{[(4\eta-2)\alpha+\eta(1+\eta)\eta+(1-\eta^2)]/(5\eta-1)} \times t_0^{3(1-\eta)(\alpha-1+\eta-\eta\eta)/(5\eta-1)} \times t^{\eta[(1-\alpha)+(4\eta-1)(1-\eta)]/(5\eta-1)} \times E^{-[\alpha+(4\eta-1)\eta+\eta-1]/(5\eta-1)}$$

$$(E_c<E<E_b).$$

.....(5.A1.11)

After $t = t_*$, $E_b > E_{max}$; and the entire particle spectrum evolves adiabatically. Absence of injection above E_{max} modifies the particle distribution above an energy $\bar{E} \equiv E_{max}\left(t_*/t\right)^{\eta}$. The energy spectrum above $\bar{E}$ is given by

$$N(E,t) = \frac{(2-\alpha)\epsilon_p L_0}{(\alpha-1)-\eta(\alpha-1)} \tau_0^{\alpha} E_{max}^{(\alpha-1-\eta)/\eta} t^{1-\alpha} E^{(1-\eta-\alpha)/\eta}$$

$$(E > \bar{E})$$

.....(5.A1.12)

and (5.A1.11) gives the spectrum between E_c and $\bar{E}$.

If at $t = \tau_0$. E_b is already higher than E_{max}, then in phase III the spectrum consists only of two sections, given by (5.A1.10) for energies $E < \tilde{E} \equiv E_{max} (t/\tau_0)^{-\eta}$, and by (5.A1.12) for $E > \tilde{E}$

Case B:

In this case. expansion in phase II is undecelerated, and hence is described by the expressions derived in appendix 2.A2. Modifications are necessary only in phase III.

Phase III

At times $t < t_0$. the field and particle distribution will be as described in appendix 2.A2. At $t > t_0$. the magnetic field is given by

$$B(t) = \left[\frac{3\alpha\epsilon_m L_0}{(\alpha-2)v^3}\right]^{1/2} \tau_0 t_0^{2(\eta-1)} t^{-2\eta}. \quad (5.A1.13)$$

The break energy

$$E_b = \frac{\eta(\alpha-2)v^3}{3\alpha\epsilon_m c_1 L_0 \tau_0^2} t_0^{4(1-\eta)} t^{4\eta-1} . \qquad (5.A1.14)$$

For $E > E_b$,

$$t_i \simeq t, \text{ and } \frac{\partial t_i}{\partial E} \simeq \frac{(\alpha-2)v^3 t_0^{4(1-\eta)}}{3\alpha\epsilon_m c_1 L_0 \tau_0^2} \frac{t^{4\eta}}{E^2}$$

which gives

$$N(E,t) = \frac{(2-\gamma)(\alpha-2)}{3\alpha(\gamma-1)c_1} \cdot \frac{\epsilon_p}{\epsilon_m} \cdot v^3 E_{max}^{\gamma-2} \tau_0^{\alpha-2} t_0^{4(1-\eta)} \times t^{4\eta-\alpha} E^{-(\gamma+1)}$$

$$(E > E_b) . \qquad .....(5.A1.15)$$

At $t = t_0$, the spectrum of adiabatic loss dominated "relic" particles is as follows.

a) $$N(E,t_0) = \frac{\alpha(2-\gamma)}{\gamma(\alpha-\gamma)} \epsilon_p L_0 E_{max}^{\gamma-2} \tau_0^{\gamma} t_0^{1-\gamma} E^{-\gamma}$$

$$\text{for } E < E_c(t_0) \equiv E_b(\tau_0) \frac{\tau_0}{t_0}$$

and

$$b)\quad N(E,t_o) = \frac{2-\eta}{\alpha-\eta}\left(\frac{\alpha-2}{3\alpha\epsilon_m c_1}\right)^{(\alpha-\eta)/4} \epsilon_p^{\,(4-\alpha+\eta)/4} L_o^{\,\eta-2} E_{max}^{\,\eta-2} \times v^{3(\alpha-\eta)/4} \tau_o^{\,(\alpha+\eta)/2} t_o^{\,(4-\alpha-3\eta)/4} \times E^{-(\alpha+3\eta)/4}$$

$$\text{for } E_c(t_o) < E < E_b(t_o)$$

at $t > t_o$, type a) relic particles will be found below the energy $E_c(t) = E_c(t_o)\,(t/t_o)^{\eta}$; and type b) relic particles will remain in the energy interval $E_c(t) < E < E_d(t) \equiv E_b(t_o)(t/t_o)^{-\eta}$. It can be shown that in both these regimes, i.e. for all energies below $E_d(t)$, the relic particles dominate the spectrum. Hence the low energy part of the spectrum will have these two regions:

$$N(E,t) = \frac{\alpha(2-\eta)}{\eta(\alpha-\eta)} \epsilon_p L_o E_{max}^{\,\eta-2} \tau_o^{\,\eta} t_o^{(1-\eta)(1-\eta)} t^{\eta(1-\eta)} \times E^{-\eta} \qquad (E < E_c(t))$$

.....(5.A1.16)

and

$$N(E,t) = \frac{2-\eta}{\alpha-\eta}\left[\frac{\alpha-2}{3\alpha\epsilon_m c_1}\right]^{(\alpha-\eta)/4} \epsilon_p^{(4-\alpha+\eta)/4} L_o$$

$$\times E_{max}^{\eta-2} v^{3(\alpha-\eta)/4} \tau_o^{(\alpha+\eta)/2}$$

$$\times t_o^{(1-\eta)(4-\alpha-3\eta)/4}$$

$$\times t^{\eta(4-\alpha-3\eta)/4}$$

$$\times E^{-(\alpha+3\eta)/4}$$

$$(E_c < E < E_d(t)).$$

.....(5.A1.17)

Above $E = E_d(t)$, fresh particles dominate the spectrum. Between $E_d(t)$ and $E_b(t)$, particles undergoing only adiabatic losses dominate. The resultant spectrum is

$$N(E,t) = \frac{(2-\eta)\,\epsilon_p L_0 E_{max}^{\eta-2}}{(\alpha-1)-\eta(\eta-1)} \left[\frac{\eta(\alpha-2)\,v^3}{3\alpha\,\epsilon_m L_0 C_1}\right]^{\frac{\alpha-\eta\eta-1+\eta}{5\eta-1}}$$

$$\times \tau_0^{[(5\eta-3)\alpha+2\eta\eta+2(1-\eta)]/(5\eta-1)}$$

$$\times t_0^{4(1-\eta)(\alpha-\eta\eta-1+\eta)/(5\eta-1)}$$

$$\times t^{\eta[4\eta-\alpha-(4\eta-1)\eta]/(5\eta-1)}$$

$$\times E^{-[\alpha+(4\eta-1)\eta+(\eta-1)]/(5\eta-1)}$$

$$(E_d < E < E_b).$$

.....(5.A1.18)

The spectrum in the range $E_b < E < E_{max}$ is given by (5.A1.15).

. At a time t_* , the break energy $E_b(t)$ will cross E_{max}. Then onwards the evolution of the entire spectrum will be adiabatic. The absence of injection at $E > E_{max}$ will modify the spectrum above the energy $E \equiv E_{max}(t/t_*)^{-\eta}$. In the interval $\bar{E} < E < E_{max}$ the energy distribution will be given by (5.A1.12).

If at $t = t_o$, $E_b(t_o) > E_{max}$, then the relic particle spectrum will have the high-energy tail $E > \bar{E}(t_o)$ modified because of the **absence of injection above** $E = E_{max}$. **In** this case, at $t > t_o$ the second break energy E_4 will be defined as $\bar{E}(t_o)(t/t_o)^{-\gamma}$. **The spectrum** is given by **(5.A1.16)** below $E = E_c(t)$, by **(5.A1.17)** in the range $E_c < E < E_d$, and **by (5.A1.12)** for $E > \tilde{E} \equiv E_{max}(t/t_o)^{-\eta}$. **In** the interval $E_d < E < \tilde{E}$ the spectrum will have the form

$$N(E,t) = \frac{2-\gamma}{\alpha-\gamma}\,\epsilon_p L_o E_{max}^{(\alpha-2)} \tau_o^{\alpha} t_o^{(\eta-1)(\alpha-1)} t^{\eta(1-\alpha)} \times E^{-\alpha} \qquad (E_d < E < \tilde{E}). \qquad \text{.....(5.A1.19)}$$

If, on the other hand, Phase III is fully adiabatic, **i.e.** $E_b(\tau_o) > E_{max}$, then the spectrum at $t > t_o$ has three sections, given by **(5.A1.16)** for $E < E_c \equiv \bar{E}(t_o)(t/t_o)^{-\eta}$; **by (5.A1.19) for** $E_c < E < \tilde{E} \equiv E_{max}(t/t_o)^{-\eta}$; and **by (5.A1.12) for** $\tilde{E} < E < E_{max}$.

REFERENCES

Bandiera, R., Pacini, F., Salvati, M., 1984, Astrophys. J., 285, 134-140

Bhattacharya, D., Srinivasan, G., 1987, in: High Energy Phenomena Around Collapsed Stars, proceedings of NATO Advanced Study Institute (Cargese, 1985), ed. F. Pacini, D. Reidel, p.235-242

Chanan, G.A., Helfand, D.J., Reynolds, S.P., 1984, Astrophys. J., 287, L23-L26

Chevalier, R.A., 1977,in: Supernovae, ed. D.N. Schramm, D. Reidel, Dordrecht, p.53-61

Chevalier, R.A., 1978, Mem. Soc. astr. Ital., 49, 497-511

Clark, D.H., Green, A.J., Caswell, J.L., 1975; Aust. J. Phys. Astrophys. Suppl., No. 37, 75-86

Clark, D.H., Tuohy, I.R., Long, K.S., Szymkowiak, A.E., Dopita, M.A., Mathewson, D.S., Culhane, J.L., 1982, Astrophys. J., 255, 440-446

Cowie, L.L., Songaila, A., 1986, Ann. Rev. Astr. Astrophys., 24, 499-535

Cowsik, R., Sarkar, S., 1984, Mon. Not. R. astr. Soc., 207, 745-775

Davelaar, J., Smith, A., Becker, R.H., 1986, Astrophys. J., 300,. L59-L62

Duin, R.M., Strom, R.G., 1975, Astr. Astrophys., 39, 33-42

Gull, S.F., 1973, Mon. Not. R. astr. Soc., 161, 47-69

Gull, S.F., 1975, Mon. Not. R. astr. Soc., 171, 237-242

Heiles, C., 1980, Astrophys. J., 235, 833-839

Higdon, J.C., Lingenfelter, R.E., 1980, Astrophys. J., 239, 867-872

Jenkins, E.B., Meloy, D.A., 1974, Astrophys. J., 193, L121-L125

Lozinskaya, T.A., 1979, Sov. Astr., 23, 506-507

Lozinskaya, T.A., 1980, Sov. Astr., 24, 407-412

Mathewson, D.S., Dopita, M.A., Tuohy, I.R., Ford, V.L., 1980, Astrophys. J., 242, L73-L76

Mathewson, D.S., Ford, V.L., Dopita, M.A., Tuohy, I.R., Long, K.S., Helfand, D.J., 1983, Astrophys. J. Suppl. Ser., 51, 345-355

Mauche, C.W., Gorenstein, P., 1985, in: Crab Nebula and Related Supernova Remnants, ed. R.B.C. Henry and M.B.C. Kafatos, Cambridge, p.81-88

Middleditch, J., Pennypacker, C.R., 1985, in: Crab Nebula and Related Supernova Remnants, ed. R.B.C. Henry and M.B.C. Kafatos, Cambridge, p.179-186

Mills, B.Y., Turtle, A.J., Little, A.G., Durdin, J.M., 1984, Aust. J. Phys., 37, 321-357

Murdin, P., Clark, D.H., 1981, Nature, 294, 543-544

Radhakrishnan, V., Murray, J.D., Lockhart, P., Whittle, R.P.J., 1972, Astrophys. J. Suppl. Ser., 24, 15-47

Rees, M.J., Gunn, J.E., 1974, Mon. Not. R. astr. Soc, 167, 1-12

Reynolds, S.P., 1985, Astrophys. J., 291, 152-155

Reynolds, S.P., Chanan, G.A., 1984, Astrophys. J., 281, 673-681

Reynolds, S.P., Chevalier, R.A., 1984, Astrophys. J., 278, 630-648

Rogerson, J.B., Spitzer, L., Drake, J.F., Dressler, K., Jenkins, E.B., Morton, D.C., York, D.G., 1973, Astrophys. J., 181, L97-L102

Sarkar, S., 1982, Ph. D. Thesis, University of Bombay

Scott, J.S., Chevalier, R.A., 1975, Astrophys. J., 197, L5-L8

Seward, F.D., Harnden, F.R., Helfand, D.J., 1984a, Int. Astr. Union Circ. No. 3928

Seward, F.D., Harnden, F.R., Helfand, D.J., 1984b, Astrophys. J., 287, L19-L22

Shklovskii, I.S., 1980, Publ. Astr. Soc. Pacific, 92, 125-126

Spitzer, L., 1956, Astrophys. J., 124, 20-34

Spitzer, L., 1978, Physical Processes in the Interstellar Medium, Wiley, New York

Spitzer, L., 1982, Searchins between the stars, Yale, U.S.A.

Srinivasan, G., 1985a, in: Supernovae, their Progenitors and Remnants, ed. G. Srinivasan and V. Radhakrishnan, Indian Acad. Sci., Bangalore, p.105-117

Srinivasan, G., Bhattacharya, D., 1984, Curr. Sci., 53, 513-516

Srinivasan, G., Dwarakanath, K.S., 1982, J. Astrophys. Astr., 3, 351-361

van der Laan, H., 1962, Mon. Not. R. astr. Soc., 124, 179-187

Velusamy, T., 1985, in: Crab Nebula and Related Supernova Remnants, ed. R.B.C. Henry and M.B.C. Kafatos, Cambridge, p.115-126

Weiler, K.W., 1983, in IAU Symp. 101: Supernova Remnants and Their X-ray Emission, ed. P. Gorenstein and J. Danziger, D. Reidel, Dordrecht, p.299-320

Weiler, K.W., 1985 , in: Crab Nebula and Related Supernova Remnants, ed. R.B.C. Henry and M.B.C. Kafatos, Cambridge, p.227-239

Weiler, K.W., Panagia, N., 1980, Astr. Astrophys., 90, 269-282

Wilson, A.S., 1972, Mon. Not. R. astr. Soc., 157, 229-253

York, D.G., 1974, Astrophys. J., 193, L127-L131